Allanites in the Sin Quyen IOCG deposit, North Vietnam

Chau Nguyen Dinh[1], Jadwiga Pieczonka[1], Adam Piestrzyński[1,*], Phon Le Khanh[2], Hao Duong Van[2]

[1] AGH University of Science and Technology; cnd@agh.edu.pl; jpeczon@agh.edu.pl; piestrz@agh.edu.pl
[2] Hanoi University of Mining and Geology; lekanhphon.humg@gmail.com; haodnth@gmail.com
[2] *Correspondence: piestrz@agh.edu.pl;Tel.: +48 12 6172433

Abstract: Allanite minerals are the principal host of REEs in the Sin Quyen, Iron Oxide Copper Gold (IOCG) type deposit. The studied allanites have concentrations of: REE (14-27 wt%), Ca (9-16 wt%), Al (8-19 wt%), Si (26-34 wt%) and Fe (12-21 wt%). Two populations of allanite are documented, the first is texturally older probably related to the Ca-K alteration (second stage of crystallization). This population has higher REE concentrations ranging from 20 to 27 wt%, and the second population texturally younger has lower total REE concentration ranging from 14 to 19.9 wt%, which occur as a rim surrounding the older and likely arose during the K alteration with Cu-Au mineralization (third crystallization). Differences between the two allanite populations are documented by both optical properties and analysis of their chemical composition. The last parameter indicate that the studied allanites belong to the Ce-La-ferriallanite family, with low ΣHREE with an average of 0.21 wt.%. Temperature 355ºC which was calculated using value of $\delta^{34}S$ isotopes is interpreted as a temperature of the second crystallization stage of allanite. The pressure of crystallization solution was calculated and is ranging from 0.98 to 5.88 MPa.

Keywords: allanite**;** REE; ore minerals; IOCG deposit; North Vietnam

1. Introduction

Four economic to sub-economic deposits (Sin Quyen, Muong Hum, Nam Xe and Dong Pao) with above crustal average abundance of Cu, Au, Ag and REE have been identified in North Vietnam [1]. The Sin Quyen deposit is the largest IOCG deposit in this area and is actively mined. The copper grade in the ore ranges from 0.55 % to 1.93 %, and the abundance of iron ranges from a few percent up to several tens of percent [1-3]. The ore reserves of this deposit are reported as 550,000 t Cu, 334,000t REE, 843,000 t S, 34.7t Ag and 25.3 t Au [4-7]. Since 2006 the deposit has been exploited with an open cast system and the Fe- and Cu-concentrates are produced by magnetic and gravity flotation respectively. However, the Fe-concentrate is not economic. The annual production of over 30,000 tons of Cu, and approximately 300 kg Au as coproduct are reported, but REE have not been recovered.

The major ore bearing minerals identified in the deposit are magnetite, pyrite, pyrrhotite, chalcopyrite, cubanite, and sphalerite. Allanite, ilmenite, marcasite, tennantite, arsenopyrite and galena are accessory minerals, and native-Bi, bismuthinite, electrum, native gold, uraninite, and tellurides as minor constituents. The Sin Quyen deposit is interesting from scientific point of view, since it consists of a complicated spatial distribution of various commodities and multi crystallisation stages as suggested by the results of absolute dating techniques [3,5,7]. Due to the overlap of magmatic, hydrothermal and metamorphic processes resulting in several crystallization stages in the deposit, origin, ore crystallization,

and relationships between the major and minor elements and mineralisation are still being discussed [1, 5-7].

Allanite is the major REE carrier in the Sin Quyen IOCG deposit; bastnäsite and monazite are scarce. The REE-carrying minerals are dispersed but common occurring in the deposit and are found in an assemblage with amphibole and epidote in massive ore [2]. According to McLean [6] and Li and Zhou [8] the first allanite population of mineralization was accompanied with Ca-K alteration (stage II), while the second population of allanites are related to the initial stage of polymetallic ore precipitation of the polymetallic stage (stage III). The rocks hosting most of magnetite and allanite as well as sulphide extend beyond the sulphide mineralization zones [6]. McLean [6] also recognised two types of allanite; one is dark brown and more Fe rich, the other is younger, greyish in colour and surrounding the older mineral as a rim. Li and Zhou [8] and Li et al. [9] reported that REE are also contained in monazite-(Ce) and chevkinite-(Ce) in the study deposit, but with subordinate abundance. The average content of ΣLREE in the deposit is 700 ppm and dominates in the deposit [6,7,10,11], while the average content of the ΣHREE is from 9 ppm. The aims of this paper are: (i) to describe the two populations of allanite based textural occurrence, their chemical composition including in apfu; (ii) attempt to constrain the conditions of formation of the first population and second population of the allanites using $\delta^{34}S$ and other related minerals like uraninite and Cu-sulphides. Optical investigation show fine differences between two populations of allanites. Further study enables us to precisely determine nature of these phases, and statistic elaboration help to facilitate to geochemical quantitative processes.

2. Geological setting

2.1. Regional geology

In North-West Vietnam there are four structural units with NW-SE orientation: the Red River zone, Tule rift, Da River zone and Ma River shear zone (Fig.1). The Red River zone is dominated by Paleoproterozoic to Neoproterozoic-aged metamorphic and magmatic rocks including granitic gneiss, biotite–muscovite, and amphiboles [12-14]. In this zone, the Phan Si Pan and Day Nui Con Voi (DNCV) belts with ~ 10 km thick and near 300 km long form south-east part of Ailao Shan-Red River (ASRR) shear zone (Fig. 1) [13-14]. In the West close to the Red River zone there is the volcano-detrital basin Tu Le Rift bounding to the South with the Da River zone which adjacent to the Song Ma shear zone. This zone joins to the NW with Dien Bien Phu Fault in NW (Fig.1).

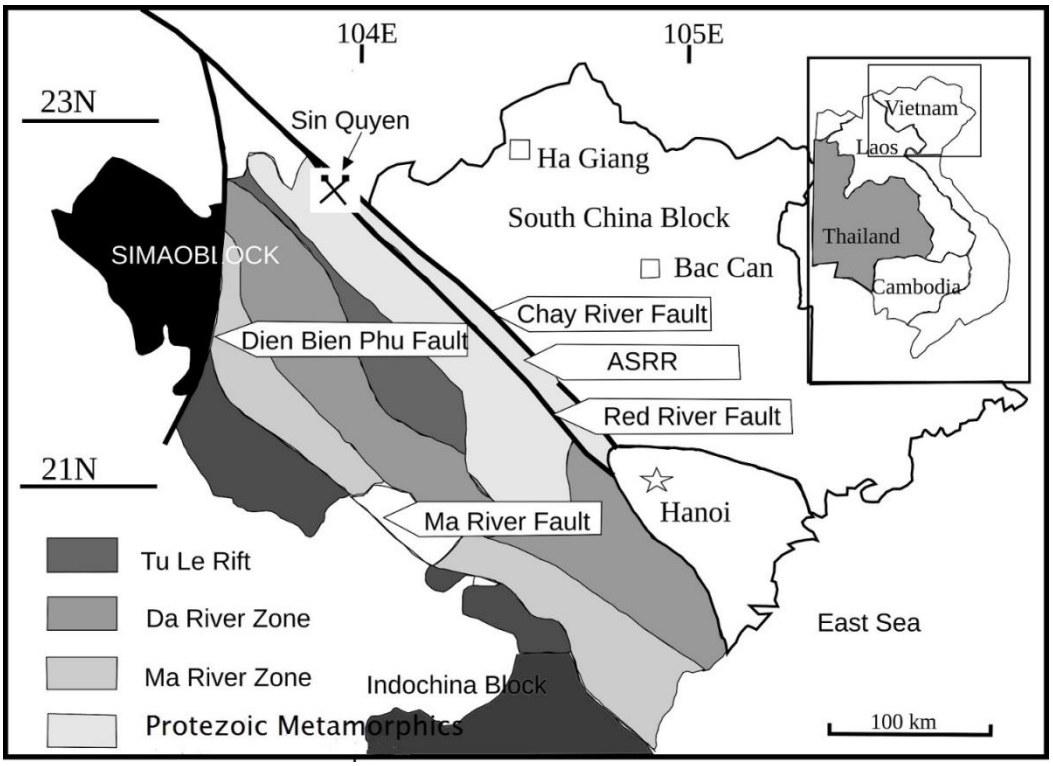

Fig. 1. Geological sketch of the Northern Vietnam with the Sin Quyen deposit localization (redrawn from [7], ASRR- Ailao Shan - Red River shear zone).

The volcanic rocks in the Tu Le rift formed during two periods: in Middle Jurassic (176 – 145 Ma) and the Late Cretaceous (80-60 Ma) [15]. The main volcanic rocks in Tu Le rift are Jurassic-Cretaceous rhyolite, trachyte and basalt, while gabbro, syenite, granosyenite and alkaline granite are minor. Da River zone is interpreted as a continental rift dominated by Trassic terrigenous calcareous and sandstone. In these formations some Permian rhyolite and tuff are interbedded. The Ma River zone consists of several northwest faults. This zone is built by Cambrian – Lower Ordovician metasediment Song Ma and Ham Rong Formations [16]. The Ma River zone has been interpreted as the boundary of the Indochina and South China blocks.

In North-West Vietnam there are several Neo-Proterozoic and Late Permian and Early Triassic igneous formations. The metamorphic processes occurred in the Red River zone could be related to several magmatic intrusion and tectonic activities. The older Proterozoic intrusive suite (~750 Ma) comprises amphibolites and granitic gneiss, intruding both Suoi Chieng and Sin Quyen formations [6-9]. This intrusive formation occurs as small lensoidal bodies in strike and dip with thick of 10-100 metre. In the Phan Si Pan Massif was formed by per-alkaline and meta-aluminous Po Sen-Hoa Binh plutons at 253-251 Ma of ages [17,18]. These magmatic bodies intruded Suoi Chieng formation (Fig. 2). In the Da River zone there is occurrence of Tu Le massif formed in the middle-late Jurassic (176-145 Ma) and late Cretaceus (80-60 Ma) [17, 18]. The main tectono-metamorphic activity of the Ma River shear zone is to the Indosinian orogeny at ~250 Ma [18-19].

Day Nui Con Voi Belt appears as elongated NW trending core of metamorphic rocks including garnet- biotite-sillimanite gneiss and garnet-biotite gneiss. This belt also consists of metamorphism amphibolite beds, migmatite, mylonite bands and small marble lenses [19]. The rocks are strongly foliated. The foliation is parallel to the local trend of the gneiss core dipping near 70° to the northeast.

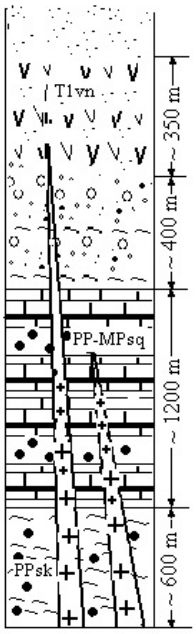

Fig. 2. Litho-stratigraphic column of the Sin Quyen area.

PPsk- Suoi Chieng metamorphosed sequence (granite, gneiss an biotite schists)– Paleo Proterozoic, PP-MPsq- Sin Quyen unit (graphite schists, mica schists, gneiss) - Tlvn – Cam Duong Formation – (marbles, limestone) Cambrian age [2, 6].

The Phan Si Pan Belt is a high-grade metamorphic complex including the Suoi Chieng, Sin Quyen and Cam Duong formations. The Suoi Chieng Formation is composed of Paleoproterozoic biotite schist, amphibolite. This formation is conformably overlain by the Paleoproterozoic to Neoproterozoic-aged Sin Quyen metamorphosed Formation comprising gneiss, mica schists and marble lenses and volcanics. Based on the mineral assemblage, the Sin Quyen Formation is divided into upper and lower units (Fig. 2).

The lower unit is dominated by graphitic schist and in the upper unit, gneiss is prevailing [5, 6]. The Sin Quyen upper formation is contacted in fault with the Cam Duong Formation, which outcrops on the surface (Fig. 2). This formation is composed of Cambrian sediments hosting apatite deposits [5,6].

2.2. *Deposit geology*

The Sin Quyen copper deposit is hosted in the Upper Sin Quyen Formation and located 300 km north-west of Hanoi, one km from the Chinese border on the east bank of the Red River. Mineralisation occurs in lenses within an elongate NW trending zone 100 – 200 m wide, nearly 2.5 km long and extending in depth to around 500 m [5]. The main mineralisation zone is strongly deformed with fractured and dislocated gneiss, mica schist and clay matrix breccia. The gneiss is principally composed of biotite, feldspar and quartz, the main composition of mica schist is biotite, muscovite, quartz and feldspar. In the mineralisation zone there are some Proterozoic granite dykes. The intrusive suites are barren of ore and basically consist of albite, biotite, and quartz [6].

The deposit is comprised of 17 lensoidal ore bodies, striking NW-SE, dipping nearly vertically (70°- 90°), several to tens of metres thick (Fig. 3), and up to a few hundred metres long (Fig.4). Following types of ore are occurring in the deposit: massive, banded, breccia cement and dispersed. Spatial distribution of Fe, Cu and REE is highly variable. From the ore geology point of view, the deposit is divided into two zones. The first zone is principally located in the central and eastern parts, and the main minerals are chalcopyrite, pyrrhotite and pyrite, which constitute nearly 90 % of the ore composition with broad variations in content at different sites. The second zone dominates in the western part; its principal minerals are magnetite, pyrite, chalcopyrite and pyrrhotite. The minerals contain from a few percent to 50 % or more of the ore composition. In the study deposit, allanite is the major carrier mineral for REE, bastnäsite, apatite and monazite are scarce [2,5,6]. To the REE-bearing minerals belong also titanite, epidote and uraninite [20]

Fig. 3. Mining section with position of the ore body (black rocks) marked with red lines (view towards NW, photo 2014).

3. Samples and analytical methods

3.1.Samples

The samples used encompass a broad range of geological materials available in the study area: from the different sulphide by the skarn, massive and breccia ores up to Cu, Fe concentrate and ore enrichment waste. The short description of some sample is provided in the Table 1. The locations of the samples were determined using a Garmin 60CSx GPS, with an accuracy of ± 2-3m and are shown on Fig. 4. From the spatial distribution of view, the 34 samples were collected from all zones in the deposit. The samples M1-M8 were collected from the central part, samples N1-N12 from the northern and S1-S9 from the southern part.

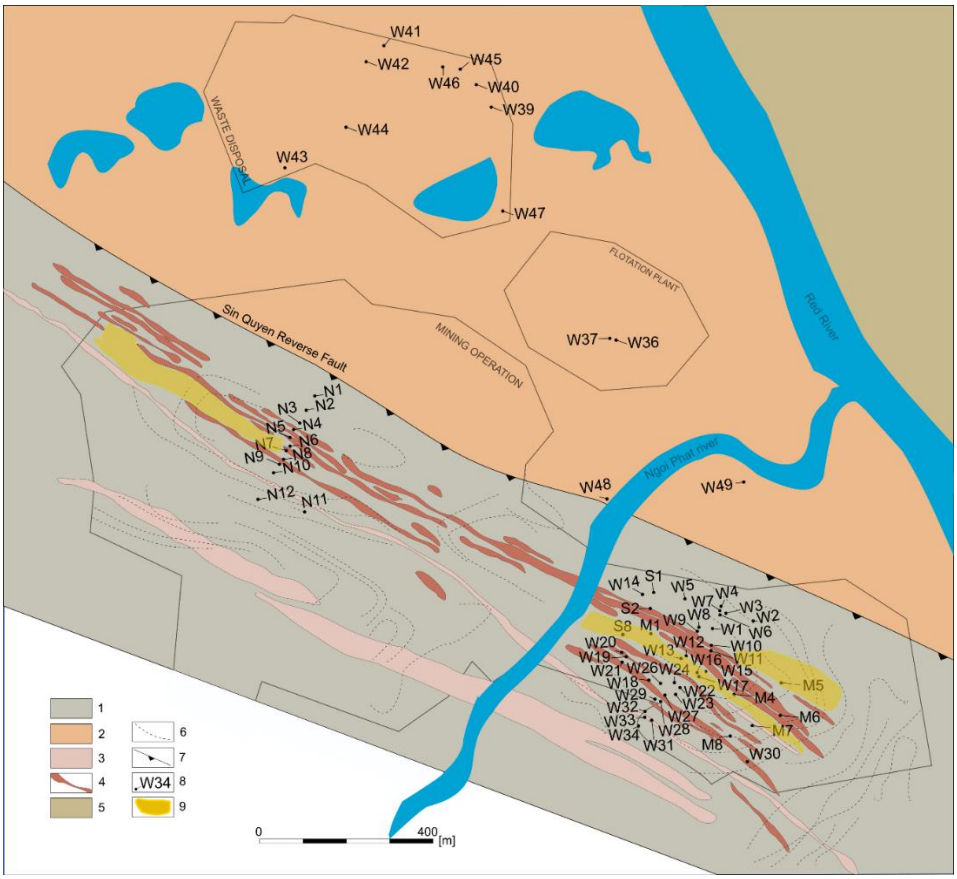

Fig.4. Geological map of the Sin Quyen deposit with location of studiet samples (adopted from [7] and [2] 1- leucocratic biotite, plagioclase, K-feldspars –quartz, Paleo Proterozoic sequence, 2- Cambrian metasedimentary rocks; 3- biotite granite and granodiorite,; 4- orebody, 5- metamorphic sequence; 6- topographic lines; 7- fault and deep direction; 8- sampling; 9- alteration zone

3.2. General petrographic characteristics of the principal rocks occurring in Sin Quyen IOCG deposit

In general the Sin Quyen deposit consists of alternating leucocratic and melanocratic formations cut by lenticular pegmatoidal bodies of quartz-feldspar composition and by quartz veins up to 40 cm thick. The leucocratic rock consists mainly of quartz (35-40%), K-feldspar (15-20%), acid plagioclase (20-25%) with porphyritic texture. The melanocratic rocks contain mainly dark colored minerals: hornblende (65-70%), biotite (up to 15%), quartz (up to 35%), plagioclase (up to 30%), epidote (up to 45%) and allanite (1-3%). Quartz-amphibole-epidote rock is subordinate and occurs only within the ore hosting member. The rock is built of epidote (35-45%), amphibole (10-20%), and quartz (up to 20%). The main specific feature of this rock is a high (5-7%) allanite [5,6]. This mineral occurs in assemblage with metamorphic minerals. It concentrates basically in amphibolites, where it is assemblage with amphibole and epidote. Siltstone, gneiss and metamorphic skarn as metamorphosed sedimentary and gabro-amphibole, granite gneiss, porphyry granodiorite, porphyry granite and porphyry syenite as intrusive rocks are dominating in the study region.

3.3. Textural and compositional analysis

Analyses of ore minerals were carried out using a petrographic microscope with reflected light and a FEI Quanta-200 FEG scanning electron microscope at 20 kV acceleration equipped with EDS detector, located at the laboratories of the Faculty of Geology, Geophysics and Environmental Protection AGH-University of Science and Technology in Krakow, Poland (FGGEP AGH-UST).

Bulk chemical analyses were carried out at ACME Laboratories in Vancouver Canada using the AQ251 method. A sample of 0.5 g was digested in Aqua Regia at 90°C, followed by ICP-MS. A detailed description of the analytical methodology, detection limits, and uncertainties can be downloaded from the ACME Laboratories website at www.acmelab.com. Analytical uncertainties are typically 5% for most of the elements analysed. The detection limit for REEs varies from 0.02 ppm to 0.5 ppm, and for U and Th is equal to 0.1 ppm. The obtained chemical data were statistically processed.

3.4. REE analyses in allanites

Quantitative analyses were carried out at the Critical Elements Laboratory of the FGGEP AGH-UST using a JEOL SQ8200 electron-probe micro-analyser (EPMA). For the principal elements, the following and measurement lines and standards have been used: SiKα (albite), AlKα (kyanite), SKα (anhydrite), UMβ (UO_2), YLα (YPO_4), PKα(YPO_4), ScKα (100%), TiKα (rutile), CeLα ($CePO_4$), LaLα ($LaPO_4$), ThMα (ThO_2), CaKα (wollastonite), PrLβ (PrPO4), TbLα ($TbPO_4$), DyLα ($DyPO_4$), ErLα ($DyPO_4$), LuLα ($LuPO_4$), GdLβ ($GdPO_4$), PbMα (crocoite), NdLα ($NdPO_4$), SmLα ($SmPO_4$), EuLβ ($EuPO_4$), TmLα ($TmPO_4$), YbLα ($YbPO_4$), HoLβ ($HoPO_4$), AsLα (InAs). Overlap corrections of Nd-Ce, Sm-Ce, Lu-Dy, Dy-Eu, U-Th, Tm-Sm, Gd-Ho were carried out using the method described by [21] The EPMA was operated in the wavelength-dispersion mode at an accelerating voltage of 15 kV, and a probe current of 40 nA, with a focused beam diameter of 3 μm. Peak/background counting times [s] were as follows: Si 10/5, Al 10/5, S 20/10, U 120/60, REE 45/15, P 20/10, Ti 20/10, Th 120/60, Ca 20/10, Pb 180/90, V 10/5, Fe 20/10 and As 20/10. The Jeol ZAF matrix correction procedure was used during final quantification of all elements analyzed.

3.5. Estimation of ore crystallization temperature using sulphur isotopes

Using sulphides $\delta^{34}S$ isotopes data provided by [22] crystallization temperature was calculated. The main factors controlling a magnitude of equilibrium sulphur stable isotope fractionations are temperature, chemical composition, crystal structure and pressure [23, 24]. For the crustal condition temperature and chemical composition are the most important, but pressure effect is minimal.

For sulphides occurring in Sin Quyen IOCG deposit the measured values of $^{34}\delta S$ are 8.65 ‰ and 8.27‰ for chalcopyrite and pyrrhotite respectively [20]. Therefore $\Delta_{ch\text{-}py} = 0.38‰$. Using obtained $^{34}\delta S$ of pyrrhotite and chalcopyrite [20] and follow Ohmoto and Rye [23] the calculated crystaliazation temperature was 355 ℃

4. Geochemistry of the host rock and ore

The host rock and ore include interbedded gneisses; composed of biotite - quartz and feldspar – biotite - muscovite; quartz and feldspar mica schists; metasomatites and amphibolites, which host the mineralisation, and marbles [6]. The copper concentration ranges from several tens ppm to more than 10.0 wt% (Tab. 1) with an average of 2.56 wt% in the deposit. The iron content ranges from a single percent up to 40.0%, and reflects the combined Fe content in magnetite, silicates, pyrite and chalcopyrite (Tab. 1). Zn, Pb, Co, Ni, Mo, Sb and Se values are below 100 ppm (Tab. 1). The concentrations of Au and Ag are highly variable. Gold in the ore and rock samples ranges from a single ppb to 18.5 ppm with an average of 1.66 ppm. Silver concentrations range from 8 ppb to 4,650 ppb, with an average of 1,160 ppb (Tab. 1). High Au and Ag contents are commonly associated with massive copper ore characterised by high Cu concentration, suggesting an association of native gold with chalcopyrite and pyrite (Tab. 1). All samples are characterised by low concentrations of Ti (Tab. 1), however in some ore samples coarse crystalline titanite have been identified. The low amount of Ti is typical for IOCG deposits [25-27]. The REE element analyses in rock chip samples show elevated values in the samples with economic copper concentrations (Tabs. 1 and 2). Only three of the 34 ore samples analysed have REE values greater than 0.2 wt% (Tab. 2). The average content of the ΣLREE is 692 ppm (for n = 34; Tab. 2), while that of ΣHREE is 9 ppm (Tab. 2). The patterns of REE are presented in Figure 5.

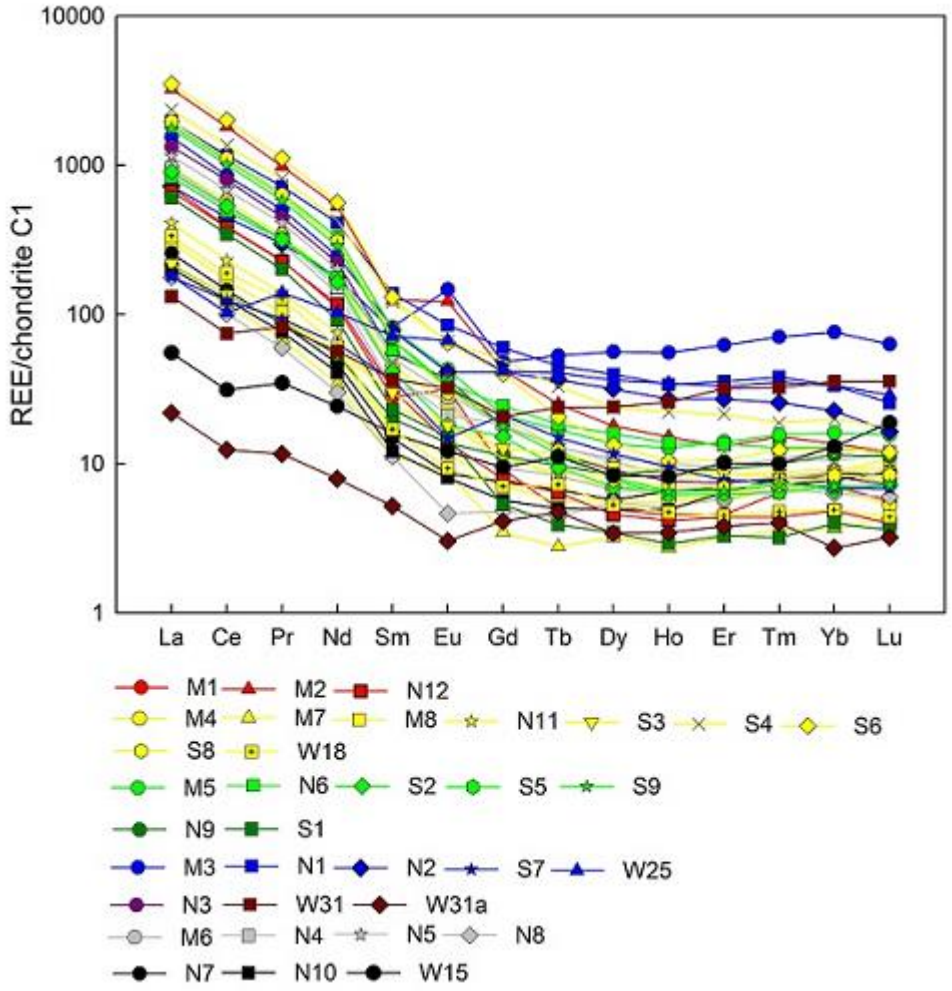

Fig. 5. REE pattern of bulk rock compositional analyses

In this figure the red color marked for the samples collected from Cu-Fe ore hosted in amphibolite, the yellow for the samples from massive ore, the green for samples for Cu-Fe banded ore, most green for metamorphic amphibolite schists, blue – amphibolite, most red for skarn rock, grey for amphibolite hosting ore and black for Cu-ore hosted in quartz-amphibolite rocks.

Generally the REE occur in all the host rocks and ore with different proportions, but all the studied materials are rich in LREE. The blue line of samples is relatively rich in the HREE (Fig. 5). The yellow group of analyzed samples represents mostly massive ore, show higher concentration of LREE. The behavior of Eu is also various, even for the samples of one type, in one sample there is negative but in other is positive suggesting the crystallization conditions in the deposit were very diverse.

Table 1. Bulk chemical compositions of samples collected from rocks and ore (ACME lab.)

sample	Na	Mg	Al	S	K	Ca	Sc	Ti	V	Cr	Mn	Characteristics of the sampling point
unit	%	%	%	%	%	%	ppm	%	ppm	ppm	ppm	
LLD	0.01	0.01	0.01	0.02	0.01	0.01	0.02	0.001	2	0.5	1	
M1	0.09	0.14	0.55	7.46	0.14	1.09	1.1	0.025	28	16	274	Ep-Am rock, Cu-Fe ore
M2	0.12	0.34	0.95	2.38	0.19	2.16	3.2	0.078	50	8.1	308	Ep-Am rock, Cu ore
M3	0.01	0.03	0.59	3.97	0.02	4.12	1.8	0.072	44	18.8	512	Ep-Am rock
M4	0.06	0.25	0.56	5.35	0.25	0.59	2	0.083	90	19.3	226	massive Cu-Fe ore
M5	0.02	1.71	2.03	1.14	2.3	2.58	3.3	0.141	104	20	528	Cu-Fe ore
M6	0.08	0.53	1.63	1.69	1.15	1.4	2.6	0.098	50	26.8	499	Bt-Am rock,Cu ore
M7	0.11	0.14	0.68	1.87	0.13	0.92	1.4	0.017	37	5	305	massive Fe ore
M8	0.11	0.69	2.13	2.58	0.48	2.37	3.7	0.058	69	9.6	1028	massive Cu-Fe ore
N1	0.07	2.77	2.82	0.91	2.81	0.57	7.5	0.254	41	23.4	330	Ep-Qtz-Pl rock
N2	0.16	0.61	0.88	0.06	0.58	1.51	3.7	0.069	10	12.6	137	Carbonate-Quartz rock
N3	0.01	3.39	4.81	2.15	3.87	1.99	5.5	0.241	99	50.3	791	Skarn
N4	0.17	0.59	2.16	2.52	1.11	1.29	6.2	0.148	65	36.7	583	Bt-Am rock, Cu ore
N5	0.03	1.52	2.28	1.85	2.21	1.04	11.9	0.191	112	30	605	Bt-Ep rock, Cu-Fe ore
N6	0.04	0.48	1.08	2.66	0.62	1.02	2.4	0.113	103	20	332	Cu-Fe ore
N7	0.2	0.91	1.99	1.14	0.76	1.46	3.4	0.116	87	26.9	414	Cb-Qtz rock, Cu ore
N8	0.05	2.64	3.79	1.12	2.55	0.3	6.1	0.167	67	117	399	Bt-Qtz-Amp rock Cu ore
N9	0.34	1.26	2.16	0.16	0.26	2.82	4.1	0.087	50	18.6	627	Amphibolite
N10	0.01	5.43	5.9	1.26	4.11	0.32	5.7	0.266	104	46.2	449	Amphibolite Cu ore
N11	0.07	1.5	2.42	2.95	0.3	1.51	2.5	0.061	78	32.5	417	Massive Cu ore
N12	0.05	1.12	3.22	0.86	2.97	0.38	3.6	0.266	87	63.8	332	Ep-Am rock, Cu-Fe ore
S1	0.03	3.35	3.57	2.22	3.3	0.46	2.4	0.199	48	25.7	521	Bt-Am schist
S2	0.03	2.57	2.19	2.23	2.84	0.49	2.2	0.116	92	4	240	Cu-Fe ore

S3	0.04	0.5	1	2.02	0.79	0.6	1.6	0.099	92	11.6	255	Massive Cu-Fe ore
S4	0.02	0.25	0.3	2.2	0.17	0.98	1.1	0.045	81	1.9	114	Massive Cu-Fe ore
S5	0.1	0.45	1.14	1.84	0.72	0.76	3.5	0.111	73	28.4	272	Cu-Fe ore
S6	0.11	0.46	0.93	2.43	0.43	1.56	2.8	0.074	73	15.8	244	Massive Cu-Fe ore
S7	0.05	0.29	0.79	0.07	0.2	0.49	2.1	0.015	67	6.9	156	Carbonate-Quartz rock
S8	0.04	0.68	1.8	1.75	1.38	0.65	3.5	0.17	15	25.9	334	Massive Cu-Fe ore
S9	0.08	0.34	0.81	2.05	0.51	0.64	1.8	0.077	138	19.1	173	Cu-Fe ore
W15	4.22	1.03	8.52	0.1	1.34	6.72	9	0.283	61	-	1085	ore, open pit
W18	0.56	0.55	1.5	4.19	0.22	0.55	5	0.075	51	-	319	massive ore
W25	1.22	1.6	6.21	1.7	0.29	3.23	22	0.303	123	-	758	epid-amph rock
W31	1.03	3.61	4.58	0.41	1.07	6.04	16	0.268	50	-	1479	Skarn
W31a	0.02	0.26	1.95	<0.02	0.02	29.1	1	0.012	74	-	1264	skarn with garnet
Min	0,01	0,03	0,30	0,02	0,02	0,30	1,00	0,01	<2	1,90	114,0	
Max	4,22	5,43	8,52	7,46	4,11	29,10	22,00	0,30	138.00	117,00	1479,0	
Average	0,28	1,24	2,29	1,98	1,18	2,40	4,58	0,13	100.0	25,55	479,71	

Table 1 c.d.

sample	Fe	Co	Ni	Cu	Zn	Ga	Ge	Rb	Sr	Y	Nb	Ag	Cd
unit	%	ppm	ppm	ppm	ppm	ppm	ppm	ppm	ppm	ppm	ppm	Ppb	Ppm
LLD	0.01	0.1	0.1	0.01	0.1	0.1	0.1	0.01	0.5	0.01	0.02	2	0.01
M1	25.52	328.7	240.3	11539	40.9	4	0.3	2.5	8.5	6.65	0.74	508	0.18
M2	7.74	47.6	21.4	32225	85.9	5.5	0.4	4.9	48	20.41	1.5	1188	0.39
M3	18.34	225.3	220.7	6751	21.6	5.1	0.7	3.8	20.9	81.39	2.49	216	0.1
M4	29.14	119.7	43.4	44900	67.9	11.4	0.6	24.5	11.3	9.49	2.55	1344	0.45
M5	28.45	82.3	22.7	29700	50.3	17.8	0.8	115	102.1	17.2	2.03	1075	0.23
M6	13.36	57.2	27.4	26524	187.1	10.7	0.5	56.8	19.3	9.12	1.27	711	0.7
M7	31.35	71.8	37	4972	38.8	14.7	0.9	4.3	12.3	4.24	0.33	211	0.12

M8	24.28	123	58.5	10914	137.8	22.1	0.7	58.2	32.2	8.32	0.28	506	0.32
N1	4.31	24.1	18.7	8811	33.3	10.7	0.4	112	13.2	46.83	0.26	1034	0.12
N2	1.18	4.5	10.3	404	9.1	4	0.1	24.4	17	38.6	0.26	98	0.03
N3	12.26	74.5	43.6	7695	48.4	22.9	0.7	194.2	26.8	11.97	1.2	754	0.1
N4	13.21	57.3	23.1	16976	173.5	15.9	0.6	107.7	9.7	14.87	1.14	1475	1.46
N5	25.62	78.8	35.4	37861	118.2	16.4	0.7	114.4	16.3	13.33	1.47	1569	0.68
N6	25.97	140.4	57.1	74400	195.9	13.8	0.6	39.1	27.7	17.85	0.72	4159	1.58
N7	7.66	44.8	23.9	17769	48.4	10.6	0.4	37.8	16.4	9.57	0.37	581	0.25
N8	11.13	67.2	40.9	20614	59.1	15	0.3	112	6.6	7.43	0.34	488	0.26
N9	6.43	16.8	9.7	1302	26.4	9.1	0.4	10.3	20.6	13.91	0.27	83	0.06
N10	12.89	86.9	35.2	28309	96.4	23.1	0.3	178.5	5.7	8.2	1.11	952	0.49
N11	14.17	151.2	94.7	82400	145.8	11.7	0.3	20.4	17.8	10.17	0.43	3050	1.02
N12	20.72	41.2	18.5	11258	51.8	15.5	0.5	150	8.3	7.09	0.98	498	0.15
S1	10.21	61.2	45.6	3447	91.6	13.5	0.4	294.2	8.5	4.99	0.58	283	0.21
S2	21.55	128.6	32	21709	82.6	15.9	0.7	170	17.7	10.4	1.73	1668	0.72
S3	31.55	140.5	39.4	51806	182.2	13.4	0.7	59	8.7	11.42	1.55	2311	1.17
S4	30.6	182.2	91.3	107878	152.2	9.7	0.6	9.4	25	30.56	1.41	4646	0.7
S5	21.02	60	24	26150	77.9	9.6	0.5	45	22.2	9.55	1.95	1090	0.38
S6	21.53	139.9	51.7	76083	109.9	7.7	0.5	24.7	43.7	17.35	1.5	2939	0.57
S7	2.08	156	4.9	394	12.6	6.2	0.1	14.9	6.7	14.18	0.08	30	0.01
S8	26.06	334	28.6	19988	43.8	18.6	0.7	88.4	16.2	11.06	0.71	1844	0.11
S9	23.59	173	41	58040	104	8.1	0.4	30.8	21.4	10.18	1.59	2107	0.67
W15	2.73	1085	7.3	186	32.5	-	-	-	90.8	17	-	8	0.06
W18	>40	319	41.4	>10000	88.3	-	-	-	11.4	10	-	1836	0.41
W25	5.81	758	35.7	2935	34.1	-	-	-	128	66	-	139	0.11
W31	15.28	1479	9.4	3067	57.7	-	-	-	22.3	52	-	113	0.03
W31a	0.86	1264	<0.1	39	33.3	-	-	-	98.2	11	-	14	0.07

Min	0.86	114,0	4,90	39,00	9,10	4,00	0,10	2,50	5,70	4,24	0,08	8,00	0,01
Max	40.00	1479,0	240,30	107878,00	195,90	23,10	0,90	294,20	128,00	81,39	2,55	4646,00	1,58
Average	17,25	479,71	46,51	25668,06	80,57	12,51	0,51	72,66	28,28	18,60	1,06	1162,59	0,41

Table 1. c.d.

sample	Sn	Te	Cs	Ba	Au	Tl	Pb	Bi	Th	U
unit	ppm	ppm	ppm	ppm	ppb	ppm	ppm	ppm	ppm	ppm
LLD	0.1	0.2	0.5	0.5	0.2	0.02	0.01	0.02	0.1	0.1
M1	17.8	1.53	0.22	7	502.6	0.06	2.79	0.98	0.9	3.1
M2	25.3	1.5	0.38	6.7	511.1	0.06	3.79	1.47	3.3	10.5
M3	67.3	1.52	0.8	4	107.6	0.02	4.98	1.23	1.7	7.1
M4	19.6	3.53	3.34	13.4	991.8	0.21	7.01	2.85	1.4	24.7
M5	14.8	1.71	6.72	170	343.5	0.57	17.53	1.22	3	174
M6	22.7	1.06	3.14	130	237.5	0.34	5.29	0.5	1.2	10.4
M7	21.1	1.15	0.41	10.9	59.3	0.03	2.49	0.28	0.5	2.2
M8	17.1	2.42	5.5	88.2	138	0.18	3.7	0.8	0.9	3.1
N1	17.7	0.63	10.85	197	657.3	0.56	1.64	1	8	6.8
N2	3.5	0.02	2.38	53.8	102.3	0.12	1.5	0.04	5.7	5.6
N3	18.1	1.04	26.32	247	132.3	1.28	2.38	1.4	3.3	14
N4	27.1	1.99	16.93	128	1204.4	0.87	3.77	1.16	3.1	19
N5	21.3	2.57	5.58	155	462.9	0.72	3.13	2.14	1.8	3.2
N6	37.9	5.52	2.6	80.6	12687.5	0.46	33.92	3.81	3.7	513.1
N7	20.2	0.87	3.03	112	727.7	0.23	1.94	0.73	1.1	8.1
N8	8.8	0.62	8	241	161.9	0.62	3.41	0.36	3.1	56.2
N9	21.6	0.08	1.36	21.3	88.9	0.07	1.31	0.05	3.9	4.2
N10	9.3	1.36	21.27	284	175.9	1.1	2.8	1.44	2.7	31.6
N11	20.8	4.44	2.27	34.2	18503.7	0.42	24.27	4.64	3.2	302.4
N12	5.6	1.14	14.41	364	598.1	0.88	3.84	0.84	2	31.6

S1	18.5	0.66	48.69	159	121.2	1.88	3.07	0.73	2.1	8.9
S2	10.4	1.32	11.22	104	407.8	0.72	3.56	2.36	3.2	28.1
S3	36.3	4.18	6.52	57.6	294.7	0.38	26.21	3.01	1.9	331
S4	24.1	7.13	1.01	12.9	10531.2	0.08	24.6	4.67	3.8	316.8
S5	14	1.54	3.61	74.8	681.2	0.21	6.09	1.16	2.7	51.7
S7	18.5	3.95	1.51	32.4	2038.6	0.22	15.53	2.31	4.2	101.2
S8	1	0.03	0.63	20	10.4	0.06	0.89	0.06	12.5	3
S9	10.7	1.41	5.71	170	750.1	0.53	2.14	2.34	16.2	11.6
W15	13.9	3.5	2.32	48.3	897.7	0.19	10.56	2.06	21.4	74.6
W18	-	0.05	-	154	3.1	-	1.76	0.07	2.2	1.17
W25	-	3.6	-	12.8	2358.2	-	5.46	2.58	2.9	56.51
W31	-	0.28	-	18.1	28.6	-	7.61	0.31	1.4	8.35
W31a	-	0.15	-	31.4	16.9	-	3.11	0.56	0.9	16.31
Min	1.00	<0.02	0.22	4,00	1.60	0.02	0.89	0.04	0.50	0.98
Max	67.30	7.13	48.69	364.00	18503.7	1.88	33.92	4.67	21.40	513.10
Average	19.48	1.89	7.47	95.58	1662.81	0.45	7.23	1.45	3.84	65.92

Table. 2. REE bulk chemical analyses of rocks and Cu, Fe ore samples in ppm

Elements	La	Ce	Pr	Nd	Sm	Eu	Gd	Tb	Dy	Ho	Er	Tm	Yb	Lu	ΣLREE	ΣHREE	ΣREE	Marks
MDL	0.02	0.1	0.02	0.02	0.02	0.02	0.02	0.02	0.02	0.02	0.02	0.02	0.02	0.02	0.02	0.02	0.02	
M1	169.2	237.3	21.44	50.83	4.12	1.78	1.83	0.18	1.21	0.25	0.73	0.16	1.14	0.14	486.5	3.81	490.31	Ep-amph. rock. Cu-Fe ore
M2	767	1110.7	91.3	242.48	18.48	6.85	8.45	0.9	4.4	0.83	2.09	0.38	2.2	0.3	2245.26	11.1	2256.36	Ep-amph. rock. Cu ore
M3	366	522.1	47.05	112.23	12.19	8.25	9.59	1.91	13.82	3.06	9.98	1.77	12.26	1.58	1077.41	44.38	1121.79	Ep-Am rock
M4	230.4	353.5	31.52	78.51	6.77	1.4	2.29	0.29	1.74	0.32	0.9	0.17	1.13	0.13	704.39	4.68	709.07	massive Cu-Fe ore
M5	463.7	685.9	59.93	150.22	11.87	2.4	4.18	0.61	3.34	0.7	2.24	0.39	2.6	0.39	1378.2	10.27	1388.47	Cu-Fe ore
M6	208.5	314.1	27.58	63.45	4.88	1.55	1.87	0.3	1.64	0.35	1.12	0.18	1.32	0.19	621.93	5.1	627.03	Bt-amph. rock.Cu ore
M7	48.9	71.7	6.34	15.62	1.67	0.49	0.69	0.1	0.79	0.15	0.51	0.09	0.59	0.11	145.41	2.34	147.75	massive Fe ore

M8	72.8	103.1	9.58	24.17	2.44	0.65	1.42	0.2	1.39	0.3	1.02	0.16	1.41	0.27	214.16	4.75	218.91	massive Cu-Fe ore
N1	464.3	710.5	67.1	187.38	20.49	4.76	11.93	1.63	9.77	1.86	5.67	0.95	5.38	0.64	1466.46	25.9	1492.36	Ep-Qtz-Pl rock
N2	171.8	273.1	27.72	80.9	11.49	2.3	8.14	1.31	7.81	1.49	4.35	0.64	3.65	0.41	575.45	19.66	595.11	carbonate-Qtz rock
N3	315.4	488.1	41.55	102.41	8.1	2.07	3.54	0.42	2.22	0.42	1.19	0.2	1.32	0.18	961.17	5.95	967.12	skarn
N4	228.1	334	29.9	69.51	5.99	1.18	3.64	0.46	2.67	0.55	1.52	0.27	2.02	0.3	672.32	7.79	680.11	Bt-amph. rock. Cu ore
N5	272.7	417	38.04	91.91	7.51	1.66	3.50	0.47	2.54	0.46	1.48	0.26	1.7	0.29	832.32	7.2	839.52	Bt-Ep rock. Cu-Fe ore
N6	197.6	302.3	29.62	80.77	8.54	1.95	4.86	0.66	3.89	0.76	2.17	0.32	2.07	0.29	625.64	10.16	635.8	Cu-Fe ore
N7	61.1	89	8.01	21.53	2.19	0.48	1.50	0.24	1.41	0.36	1.11	0.18	1.25	0.22	183.81	4.77	188.58	Cb-Qtz rock. Cu ore
N8	42.2	61.7	5.54	13.78	1.65	0.26	0.96	0.16	1.36	0.28	0.93	0.17	1.01	0.15	126.09	4.06	130.15	Bt-Qtz-amph. rock Cu ore
N9	51.2	82.8	8.12	24.62	2.97	0.77	2.24	0.35	2.07	0.5	1.47	0.25	1.85	0.28	172.72	6.77	179.49	amphibolite
N10	48.0	77.2	7.11	18.68	1.79	0.45	1.13	0.18	1.22	0.27	1.03	0.2	1.4	0.21	154.36	4.51	158.87	amphibolite Cu ore
N11	96.9	141.2	12.99	34.32	3.55	1.02	2.16	0.31	2.06	0.45	1.35	0.22	1.49	0.23	292.14	6.11	298.25	Massive Cu ore
N12	158.4	234.8	21.2	53.4	4.66	0.78	1.57	0.23	1.12	0.23	0.7	0.11	0.78	0.1	474.81	3.27	478.08	Ep-Am rock. Cu-Fe ore
S1	143.9	211.2	18.72	41.91	3.42	0.85	1.06	0.14	0.85	0.16	0.53	0.08	0.64	0.09	421.06	2.49	423.55	Bt-Am schist
S2	215.5	326	29.66	75.06	6.17	1.01	3.02	0.34	1.72	0.36	1.08	0.19	1.06	0.18	656.42	4.93	661.35	Cu-Fe ore
S3	51.9	83.1	8.57	25.64	4.44	1.01	2.53	0.42	2.35	0.5	1.38	0.2	1.38	0.19	177.19	6.42	183.61	massive Cu-Fe ore
S4	557.1	833.7	75.64	196.2	17.95	3.69	9.80	1.19	5.82	1.22	3.44	0.47	3.2	0.44	1694.08	15.78	1709.86	massive Cu-Fe ore
S5	437.2	662.9	58.34	141.44	10.27	1.86	4.08	0.45	1.91	0.34	1	0.16	1.14	0.18	1316.09	5.18	1321.27	Cu-Fe ore
S6	831.7	1230.9	103.91	257.2	19.27	3.64	8.0	0.74	3.28	0.57	1.69	0.31	2.01	0.3	2454.62	8.9	2463.52	massive Cu-Fe ore
S7	42.2	76.4	8.64	29.07	5.42	0.83	4.20	0.54	2.88	0.52	1.24	0.19	1.11	0.17	166.76	6.65	173.41	carbonate-Qtz rock
S8	464.4	682.4	59.03	141.72	10.47	1.67	4.12	0.44	1.92	0.39	1.11	0.18	1.34	0.21	1363.81	5.59	1369.4	massive Cu-Fe ore
S9	417.1	618.4	53.93	131.1	9.97	1.81	3.55	0.42	1.98	0.36	1.05	0.18	1.14	0.18	1235.86	5.31	1241.17	Cu-Fe ore
W-15	13.1	19.13	3.24	11.09	2.36	0.68	1.89	0.4	2.05	0.45	1.62	0.25	2.1	0.47	51.49	7.34	58.83	ore from open pit
W-18	79.2	115.63	11.85	27.62	2.52	0.52	1.4	0.26	1.3	0.26	0.72	0.12	0.79	0.11	238.74	3.56	242.3	massive ore
W-25	43.1	62.92	12.98	47.01	10.58	3.74	8.31	1.46	8.93	1.9	5.28	0.88	5.38	0.72	188.64	24.55	213.19	quartz amph rock
W-31	31.2	45.55	7.67	25.95	5.45	1.8	4.11	0.86	5.9	1.42	5.11	0.81	5.72	0.89	121.73	20.71	142.44	skarn
W-31a	5.2	7.59	1.08	3.62	0.77	0.17	0.82	0.17	0.84	0.19	0.61	0.1	0.44	0.08	19.25	2.43	21.68	skarn with garnet
Min.	5.20	7.59	1.08	3.62	0.77	0.17	0.69	0.10	0.79	0.15	0.51	0.08	0.44	0.08	19.25	2.34	21.68	

Max.	831.70	1230.90	103.91	257.20	20.49	8.25	11.93	1.91	13.82	3.06	9.98	1.77	12.26	1.58	2454.62	44.38	2463.52	
Av.	**228.44**	**340.76**	**30.73**	**78.57**	**7.37**	**1.89**	**3.89**	**0.55**	**3.18**	**0.65**	**1.98**	**0.33**	**2.18**	**0.31**	**691.66**	**9.19**	**700.84**	
Std	214.56	316.80	26.79	67.70	5.51	1.81	3.04	0.46	2.95	0.63	1.98	0.34	2.22	0.29	633.29	8.74	635.68	
V [%]	97	96	90	89	77	98	80	85	95	99	103	105	105	95	94	98	93	

MDL- minimum detection limit; V- coefficient of variability

5. Deposit mineralogy

Based on an ore microscopy investigation of polished sections of the ore samples, magnetite, pyrite, pyrrhotite, chalcopyrite, and sphalerite are the major minerals, while marcasite, tennantite, cubanite, mackinawite, arsenopyrite, galena, native-Bi, bismuthinite, electrum, native gold, molybdenite, uraninite and tellurides are the minor ones. In the publication by Li and Zhou [8] chevkinite, aeschynite, bastnäsite, epidote, titanite, zircon, F-apatite and columbite are also documented. Several styles of mineralisation are recognised in the deposit: i) massive sulphide; ii) massive magnetite; iii) mixed oxide-sulphide; iv) disseminated sulphide; and v) vein hosted. All styles are characterised by different ore mineral assemblages. Based on the local distribution of the major minerals within the deposit, Gas'kov et al. [2] divided the deposit into two zones. In the first zone, which is located in the central and eastern part of the deposit, pyrite, pyrrhotite and chalcopyrite are dominant. In the second zone, which is located in the western part of the deposit, chalcopyrite and magnetite are the principal ore minerals. In magnetite-dominant ores, chalcopyrite is very common. In the massive sulphide ore, chalcopyrite, cubanite, magnetite and pyrrhotite are the major minerals. Electrum is recognised in massive sulphide ores as 1-5 μm thick fine veinlets and as 100 μm long inclusions randomly distributed in pyrite and chalcopyrite. EDS measurements of the electrum indicate an average composition of 75.7 wt% of Au, and 24.3 wt% Ag. Some Bi-S and Bi-Te minerals were also documented using the same methods. The most important Bi-S-Te mineral is tellurobismuthite containing 87.6 wt% Bi and 21.4 wt% Te. In addition to Cu sulphides, other important accompanying minerals are allanite and uraninite, which are the major carriers of REE, and U [10,11,20].

6. Results

6.1. Allanite in the deposit

Allanite is an abundant mineral in the deposit. Usually it occurs either at low concentrations, 1-2 vol%, (Figs. 6 A-E), or very rarely as a major mineral (Fig. 6F, 7). McLean [6] reported up to 85% of allanite in hastingsite-biotite-quartz metasomatites and up to 10% in skarns, while the other scientists reported that the allanite content was 5-7 vol% in skarn and 5 - 30 vol% in the ore [2, 27,28]. Based on our data, both bulk chemical analyses (Tab. 2), and the mineralogical study, the maximum content of allanite in the ore is 0.98 wt% (Tab. 2). This was calculated following the equation: av. REE content in the ore and host rock = 0.2463% (Tab. 2) multiplied by four (25% of ΣREE in allanite itself). Allanite is typically present as subhedral grains intergrown with magnetite and amphibole (Figs. 6A, B, C, D and 6F), with titanite, biotite and sulphides (Figs. 6B, and 6E) and commonly contains inclusions of these minerals. Allanites are also present as individual isometric grains and aggregates, up to 0.6 mm in size. In polished sections, grains of allanite minerals and their two populations can easily be identified in reflected light microscopy. The shadow observed on BSE pictures shows second population with lower concentration of REE in comparison with that in the first population with lighter reflect (Fig. 7). Both are usually present as intergrowths, with only a small difference in reflectivity and smoothness. The outer rim is characterized with lower reflectivity, close to the reflectivity of typical host minerals like feldspars and epidote, and depleted hardness. The contact between two phases is distinct

enough which suggests epitaxial overgrowing well visible also in transmitted light of the optical microscope.

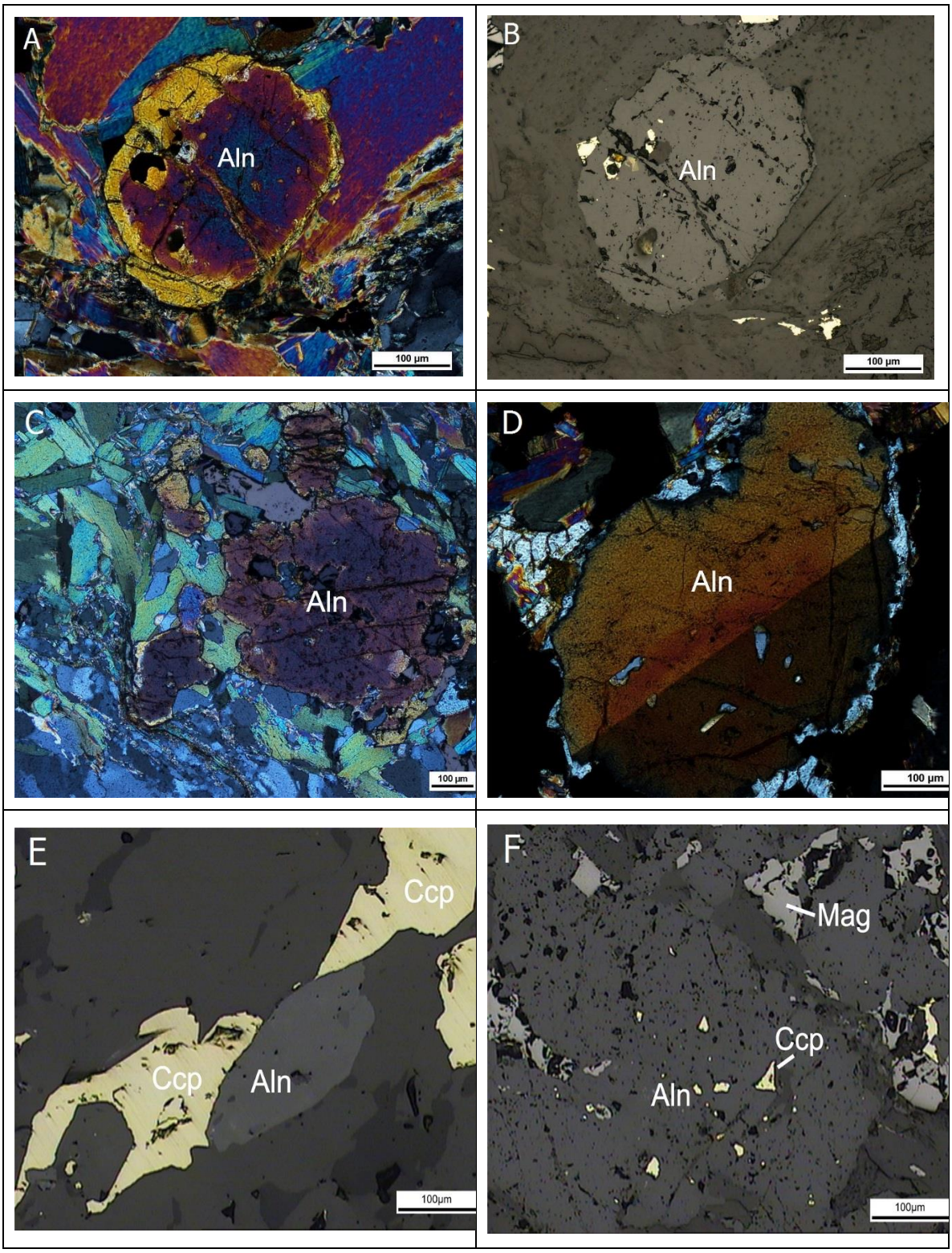

Fig.6. Microphotograph of ore minerals from Sin Quyen deposit in transmitted and reflected light.

A - allanite grain (Aln) in amphibole-biotite schist, transmitted light XN, sample N-5, B - allanite grain (Aln) in amphibole-biotite schist, white are sulphides, reflected light, sample N-5, C - allanite grains (Aln) in amphibole-biotite schist, transmitted light XN, sample N-4,

D - allanite twinned crystals (Aln) in amphibole-biotite schist, transmitted light XN, sample N-4, E - intergrowth of allanite (Aln) with chalcopyrite (Cpy), in amphibole-biotite schist, reflected light, sample W-5, F- intergrowth of allanite (Aln) with magnetite (Mgt) and chalcopyrite (Cpy), reflected light, sample W-5.

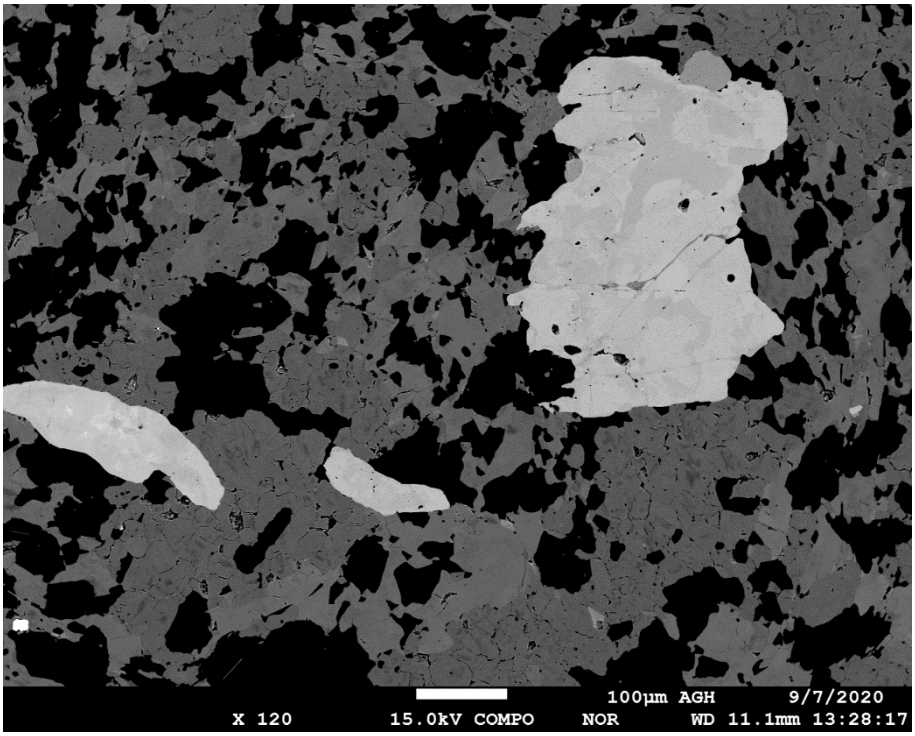

Fig. 7. BSE image of the big titanite crystal is the silicate matrix. Variable grey shadows are an effect of changings in chemical composition.

6.2 Chemical composition of allanites

WDS point measurement and WDS compositional maps (Figs. 8A - 8E and 9Al, 9Ca, 9Ce, 9La, 9Nd, 9Fe) show a high degree of compositional variability in the allanite grains. The basic chemical compositions of allanites are summarised in Tables 3a, 3b, 4a, 4b. The main characteristics of two different allanite populations are documented in Tab. 3a and Tab. 3b. The first population (core) is characterised by a high ΣREE concentration of 20 – 27 wt%, with an average 24.04 wt%, and major constituents such as Si, Fe, Al and Ca (Tab. 3a). Cerium and lanthanum are the most abundant REEs. The second population (rim) is characterised by a lower ΣREE content, ranging from 14.1 to 19.9 wt%, with an average 17.35 wt% (Tab. 3b), and by higher calcium values (Tab. 3a). The differences in allanite composition are also documented on BSE images (Fig. 8A-8F) and WDS compositional maps (Fig. ~~7~~9Al - 9Fe) also show variation in allanite compositions. The outer rim is usually depleted in Ce, La and Nd (Figs. 9Ce and 9La) and enriched in Ca and Al (Fig. 9Ca and 9Al) (rf. Tab. 3a and 3b). Iron is higher in core allanites (rf. Tab. 3a and 3b). The small (around 3 wt%) differences in Fe concentration is also shown on Figure 9Fe. However, grey tints showing Fe concentrations are not clearly visible, and show only fine differences between two allanite populations (Fig. 8). The sharp borders of the outer rim suggest two stages of allanite crystallisation. This interpretation is supported by the variable chemical composition

(Tabs. 3a ,3b and 4a and 4b) and textural development (Fig. 8A - 8F). Similar observations were also noted by McLean [6].

Table 3a. WDS composition of first population of allanite with ΣREEO higher than 20 wt%.

No.	CaO	PbO	SiO_2	As_2O_5	Al_2O_3	FeO	MgO	MnO	TiO_2	Y_2O_3	ThO_2	ΣREE	Total	Comment
1	12.4	0.02	29.0	b.d.l.	15.8	15.4	0.18	0.05	0.14	0.00	0.03	20.04	93.1	AP465_fot13_p3
2	12.4	b.d.l.	32.4	b.d.l.	15.4	15.3	0.18	0.13	0.26	0.04	0.05	20.34	96.4	AP465_fot5_p4
3	13.1	0.02	31.4	0.03	16.1	15.3	0.14	0.10	0.34	0.01	0.02	20.49	95.7	AP464 (fig.7B)
4	9.51	0.01	26.6	0.15	10.6	19.5	0.47	0.09	0.26	0.06	0.01	20.85	93.3	AP464 (fig.7B)
5	12.0	0.01	29.6	0.02	15.0	15.7	0.19	0.12	0.34	0.05	0.02	20.86	93.9	AP464_fot1_p1
6	11.8	0.01	31.2	b.d.l.	14.7	15.3	0.17	0.10	0.26	0.06	0.06	20.89	94.7	AP465_fot4_p4
7	11.5	0.02	30.8	b.d.l.	14.5	15.9	0.22	0.14	0.30	b.d.l.	0.03	21.32	94.8	AP465 (fig.7E)
8	9.14	b.d.l.	29.6	0.14	8.27	21.7	0.31	0.11	0.32	0.11	0.03	21.71	96.0	AP465 (fig.7D)
9	11.4	0.01	30.0	0.06	14.1	16.0	0.20	0.15	0.34	0.06	0.05	22.00	94.3	AP465_fot4_p5
10	11.7	b.d.l.	31.3	b.d.l.	14.6	16.4	0.20	0.12	0.26	0.01	0.02	22.34	97.0	AP465 (fig.7B)
11	10.9	0.01	27.6	0.03	13.4	17.1	0.20	0.11	0.19	0.11	0.01	22.72	92.3	AP465 (fig.7F)
12	10.8	0.01	30.7	b.d.l.	13.3	17.0	0.23	0.09	0.28	0.06	0.02	23.30	95.9	AP465_fot13_p2
13	9.34	b.d.l.	29.0	0.11	10.4	19.9	0.26	0.13	0.31	0.04	0.02	23.37	95.6	AP465 (fig. 7D)
14	10.4	0.01	30.2	0.07	12.2	17.4	0.31	0.04	0.27	0.03	0.04	23.43	94.7	AP465 (fig.7E)
15	10.6	b.d.l.	30.8	0.04	12.3	17.6	0.24	0.11	0.28	0.01	0.10	23.60	95.6	AP465_fot4_p7
16	10.8	b.d.l.	31.2	0.10	12.2	17.8	0.36	0.12	0.51	0.03	0.05	23.72	96.8	AP465_fot5_p2
17	10.5	0.01	29.3	0.03	12.6	17.1	0.27	0.12	0.21	0.05	0.14	23.97	94.5	AP465_fot4_p6
18	10.3	b.d.l.	28.9	b.d.l.	12.7	17.8	0.12	0.05	0.24	0.12	b.d.l.	24.04	94.5	AP465 (fig.7C)
19	10.3	0.01	30.0	0.21	11.4	18.3	0.41	0.07	0.08	0.03	0.02	24.18	95.0	AP465_fot4_p2
20	12.0	0.01	31.0	0.02	15.7	15.8	0.18	0.14	0.31	b.d.l.	0.01	24.31	95.7	AP464 (fig.7B)
21	10.0	0.02	29.8	0.14	11.6	18.4	0.36	0.08	0.31	0.15	0.02	24.41	95.4	AP464 (fig.7A)
22	10.1	b.d.l.	30.0	0.20	10.9	18.6	0.46	0.05	0.14	0.04	0.09	24.53	95.0	AP465_fot4_p3
23	9.14	b.d.l.	29.6	0.14	8.27	21.7	0.31	0.11	0.32	0.04	0.02	24.58	96.0	AP465 (fig.7D)
24	10.6	0.02	30.1	0.18	11.5	17.8	0.59	0.04	0.30	0.04	0.02	24.64	95.8	AP465_fot14_p3
25	13.9	0.02	29.4	0.05	17.5	14.4	0.14	0.15	0.16	0.05	0.01	24.85	93.6	AP464 (fig.7A)
26	9.84	b.d.l.	28.4	0.08	11.3	18.9	0.40	0.11	0.40	0.08	0.02	24.91	94.3	AP464 (fig.7A)
27	9.87	b.d.l.	29.2	0.17	10.8	18.5	0.51	0.05	0.18	0.07	0.05	25.04	94.5	AP465 (fig.7E)
28	10.2	0.03	30.6	0.10	10.2	19.6	0.39	0.17	0.64	0.07	0.09	25.04	97.2	AP465_fot5_p5
29	10.2	b.d.l.	28.7	0.28	11.2	18.4	0.57	0.05	0.22	0.03	0.03	25.20	94.8	AP465_fot14_p2
30	9.68	b.d.l.	30.0	0.19	11.1	18.7	0.54	0.02	0.21	0.08	0.02	25.22	95.7	AP465_fot13_p1

31	9.88	b.d.l.	28.5	0.15	10.6	18.5	0.55	0.05	0.18	0.08	0.08	25.24	93.8	AP465_fot4_p1
32	10.1	0.01	29.7	0.21	11.4	18.6	0.51	0.06	0.28	0.02	0.01	25.24	96.2	AP464_fot1_p4
33	9.88	b.d.l.	29.9	0.18	11.1	19.0	0.41	0.07	0.19	0.11	0.04	25.25	96.1	AP465 (fig.7F)
34	10.2	b.d.l.	29.5	0.27	11.3	18.6	0.50	0.05	0.27	b.d.l.	0.03	25.39	96.2	AP465_fot13_p4
35	9.90	b.d.l.	29.0	0.34	9.87	17.8	0.97	0.04	0.56	0.08	0.04	25.40	94.2	AP465_fot5_p1
36	9.81	b.d.l.	27.7	0.16	11.3	18.5	0.50	0.07	0.41	0.09	0.04	25.44	94.1	AP464_fot9_p5
37	10.0	0.02	29.2	0.18	11.0	19.1	0.42	0.09	0.24	0.05	0.03	25.5	95.8	AP465 (fig.7F)
38	9.72	b.d.l.	29.9	0.21	11.0	18.3	0.53	0.06	b.d.l.	0.03	0.05	25.57	95.4	AP465 (fig.7E)
39	12.7	b.d.l.	31.1	0.01	16.1	15.2	0.16	0.11	0.20	0.07	0.04	25.72	95.2	AP464_fot9_p3
40	10.1	b.d.l.	30.1	0.07	13.2	16.8	0.25	0.10	0.14	0.06	b.d.l.	25.79	96.5	AP465 (fig.7C)
41	9.71	b.d.l.	29.2	0.25	10.2	19.6	0.53	0.02	0.19	0.09	0.04	25.99	95.2	AP464 (fig.7B)
42	11.8	b.d.l.	30.0	0.04	14.9	15.6	0.13	0.12	0.09	0.20	0.01	26.14	94.9	AP465 (fig.7D)
43	9.49	0.02	28.2	0.18	10.5	18.9	0.55	0.08	0.48	0.04	0.03	26.34	94.9	AP464_fot1_p3
44	9.21	b.d.l.	28.8	0.15	10.5	19.5	0.32	0.14	0.13	0.00	0.04	26.36	95.5	AP465 (fig.7D)
45	11.0	0.02	30.0	b.d.l.	14.1	16.3	0.15	0.18	0.13	0.10	0.02	26.69	95.4	AP465 (fig.7D)
min.	9.14	0.00	26.6	0.00	8.27	14.4	0.12	0.02	0.00	0.00	0.00	20.04	92.3	
max.	13.9	0.03	32.4	0.34	17.5	21.7	0.97	0.18	0.64	0.20	0.14	26.69	97.2	
Av.	10.62	0.01	29.7	0.11	12.37	17.72	0.35	0.09	0.26	0.06	0.04	24.04	95.14	
St.d.	1.12	0.01	1.11	0.09	2.18	1.70	0.18	0.04	0.12	0.04	0.03	1.84	1.05	
V [%]	10.6	12.89	3.7	83.4	17.7	9.6	50.6	42.9	46.8	74.1	77.8	7.7	1.1	

Notes: Sought but not detected: U, F, S and Sc; b.d.l.- below detection limit; St.d. – standard deviation; Av- average content; V- coefficient of variability

Table 3b. WDS composition of second population of allanites with ΣREE_2O_3 lower than 20 wt%

No.	CaO	PbO	SiO_2	As_2O_5	Al_2O_3	FeO	MgO	MnO	TiO_2	Y_2O_3	ThO_2	ΣREE_2O_3	Total	Comment
1	15.618	0.004	32.576	b.d.l.	19.291	12.959	0.082	0.092	0.117	0.100	0.014	14.08	94.976	AP465_fot5_p3
2	15.444	0.020	33.370	b.d.l.	18.490	13.611	0.066	0.149	0.150	0.207	0.003	14.48	95.995	AP464 (fig.7A)
3	14.918	0.035	32.312	0.052	18.360	13.825	0.090	0.106	0.139	0.173	0.020	14.85	95.083	AP464_fot9_p4
4	14.920	0.024	31.174	b.d.l.	18.242	13.497	0.076	0.149	0.119	0.278	0.034	14.89	93.414	AP465_fot7_p3
5	14.933	0.020	33.679	b.d.l.	18.410	13.340	0.095	0.145	0.087	0.092	b.d.l.	15.53	96.329	AP465_fot1_p4

6	14.987	0.003	30.815	b.d.l.	17.889	13.711	0.073	0.150	0.178	0.148	0.048	15.38	93.283	AP465_fot14_p1
7	14.933	0.020	33.679	b.d.l.	18.410	13.340	0.095	0.145	0.087	0.092	b.d.l.	15.53	96.329	AP465_fot1_p4
8	13.868	b.d.l.	30.655	0.003	17.040	14.569	0.129	0.171	0.224	0.130	0.020	16.74	93.388	AP465 (fig.7F)
9	13.898	b.d.l.	28.854	0.098	17.377	14.147	0.124	0.149	0.154	0.077	0.027	16.93	92.015	AP464 (fig.7A)
10	10.164	0.011	29.268	0.160	11.447	18.392	0.394	0.071	0.523	0.087	0.011	17.24	95.222	AP464_fot9_p1
11	13.469	b.d.l.	30.855	0.035	16.675	14.327	0.154	0.139	0.185	0.093	0.004	17.51	93.284	AP465_fot1_p3
12	13.626	0.019	31.997	b.d.l.	16.928	14.406	0.124	0.164	0.203	0.068	0.041	17.64	95.214	AP465_fot10_p3
13	13.588	0.020	32.383	b.d.l.	17.018	14.585	0.142	0.112	0.200	0.039	0.045	17.77	96.007	AP465_fot12_p7
14	13.629	0.017	31.588	b.d.l.	17.153	14.062	0.123	0.133	0.117	0.168	0.019	17.80	94.874	AP465 (fig.7C)
15	12.924	0.024	32.067	0.066	16.225	15.206	0.146	0.190	0.246	0.160	0.018	18.72	96.089	AP465_fot10_p2
16	13.005	b.d.l.	32.056	0.078	16.387	14.741	0.138	0.071	0.144	0.089	b.d.l.	18.86	95.464	AP465 (fig.7C)
17	13.454	0.020	30.863	b.d.l.	16.984	14.219	0.119	0.142	0.193	0.219	0.010	18.86	94.650	AP465_fot10_p1
18	12.712	0.005	31.038	b.d.l.	15.853	15.173	0.146	0.149	0.269	0.048	0.036	18.93	95.200	AP464_fot10_p4
19	13.269	b.d.l.	31.997	0.006	16.679	14.586	0.111	0.143	0.198	0.186	b.d.l.	19.21	96.245	AP465 (fig.7C)
20	12.912	0.019	28.655	0.019	16.646	14.941	0.168	0.175	0.119	0.092	0.052	19.37	93.104	AP464_fot1_p2
21	13.979	0.008	31.127	b.d.l.	17.172	14.228	0.158	0.155	0.166	b.d.l.	0.009	19.39	94.366	AP464_fot9_p2
22	12.110	0.036	30.701	0.010	15.613	15.445	0.182	0.139	0.393	0.101	0.038	19.75	95.558	AP464_fot10_p3
23	12.626	b.d.l.	31.165	b.d.l.	15.956	14.831	0.165	0.113	0.151	0.119	0.023	19.89	94.875	AP465_fot12_p1
min.	10.164	0.000	28.655	0.000	11.447	12.959	0.052	0.071	0.087	0.000	0.000	14.080	92.015	
max.	15.618	0.036	33.679	0.160	19.291	18.392	0.394	0.190	0.523	0.278	0.052	19.89	96.329	
Av.	13.716	0.014	31.382	0.023	16.972	14.442	0.133	0.137	0.191	0.121	0.021	17.35	94.795	
St.d.	1.264	0.012	1.282	0.042	1.546	1.081	0.067	0.031	0.097	0.064	0.017	1.865	1.181	
V [%]	9.2	86.7	4.1	180.5	9.1	7.5	50.5	22.2	50.9	53.0	80.1	10.7	1.2	

Notes: Sought but not detected: U, S and Sc; b.d.l.- below detection limit; Av- average content; St.d.- standard deviation; V- coefficient of variability

Pearson strong correlation and high variance (R^2) between CaO, Al_2O_3, ΣFeO vs ΣREE_2O_3 (Fig. 10A-10C) suggest possible joined substitution of these elements by REE metals. The moderate variation (R^2) of SiO_2 vs ΣREE_2O_3 and the comparability of the SiO_2 amounts in both allanite populations (Tab 3a and 3b) suggest the changes in the silica composition are negligible (10D).

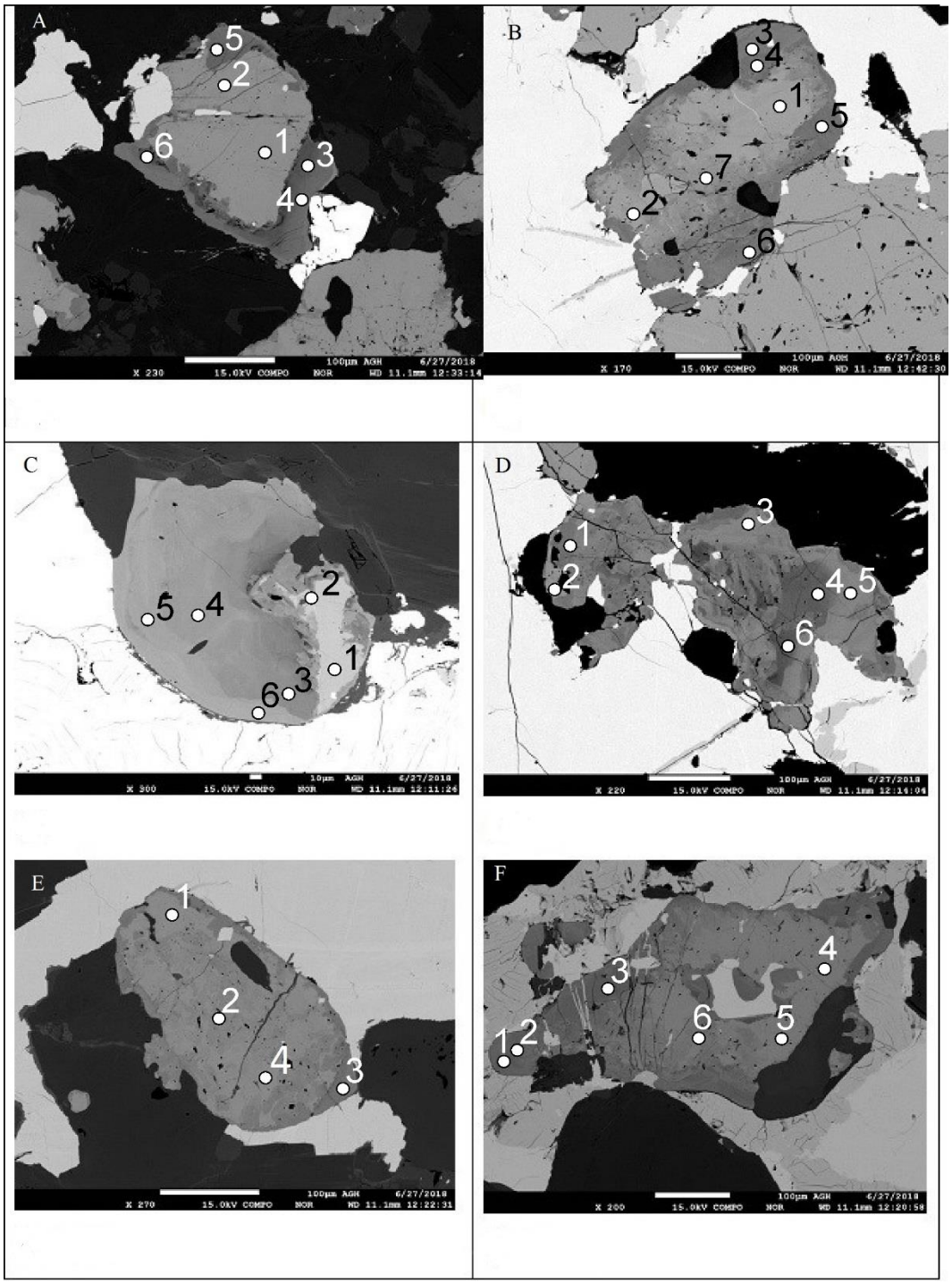

Fig. 8. Selected BSE-WDS (A-F) images of analyzed allanite grains. Gray shadows show changing in chemical composition. Numbers on pictures show positions of WDS measurements, sample N4. A- black are silicate, white-sulphides; B- white are sulphides; C- black are

silicate, white-sulphides; D- black are silicate, white-sulphides; E- black are silicate, white-sulphides; F- black are silicate, white-sulphides,

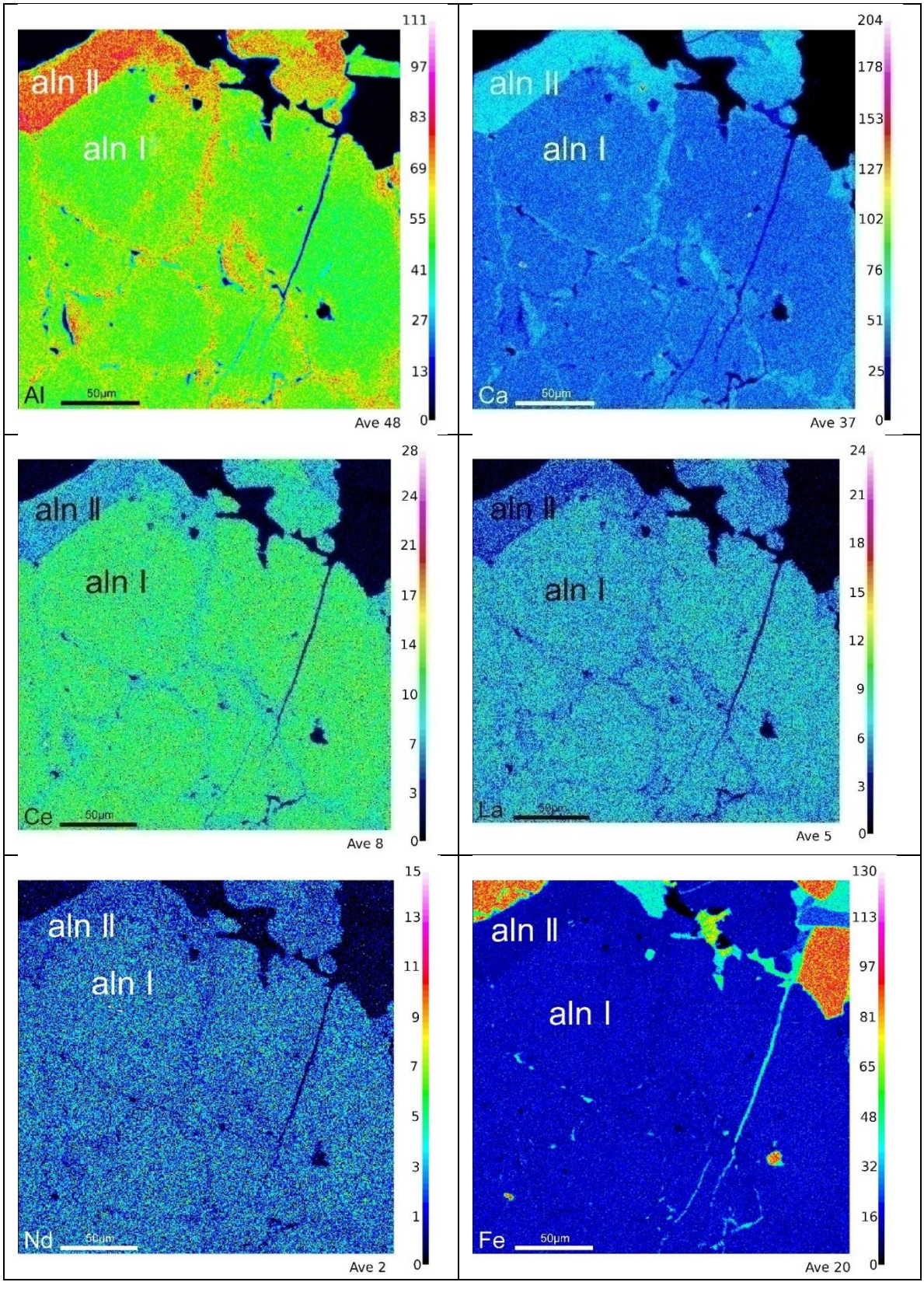

Fig. 9. WDS compositional maps of two different allanites: 9Al – contour map of Al, 9Ca contour map of - Ca, 9Ce contour map of - Ce, 9La contour map of - La, 9Nd contour map of - Nd and 9Fe contour map of – Fe

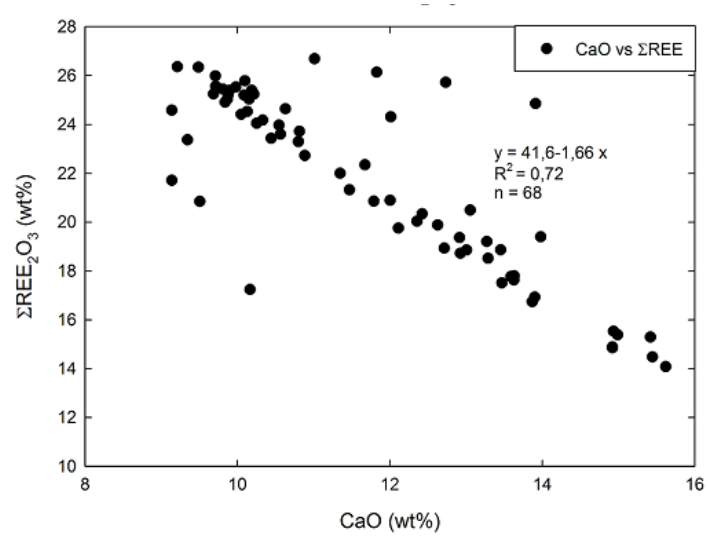

Fig. 10A. Correlation between CaO and ΣREE in allanites

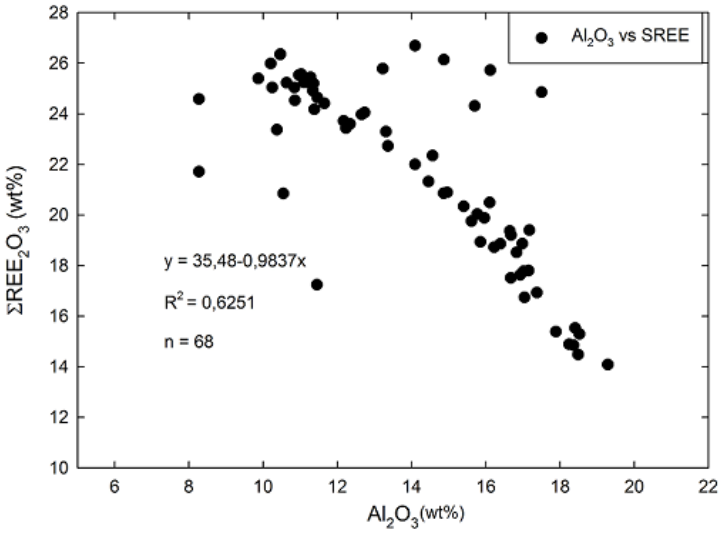

Fig.10B. Correlation between Al_2O_3 and ΣREE in allanites

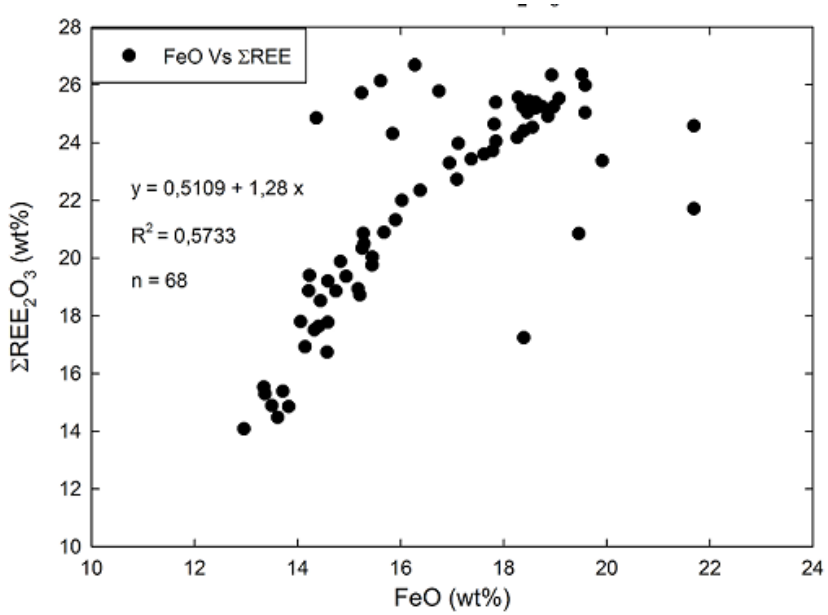

Fig. 10C. Correlation between FeO and ΣREE in allanites

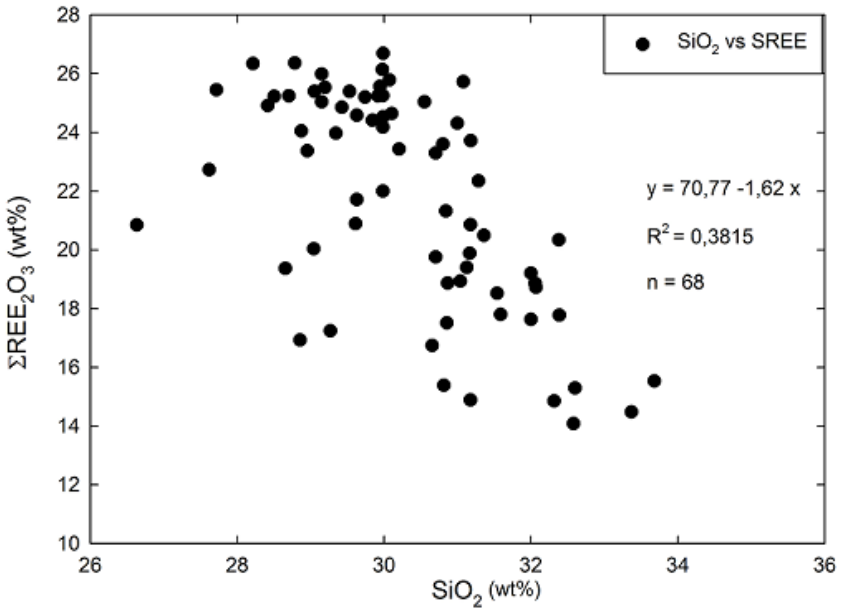

Fig. 10D. Correlation between SiO_2 and ΣREE in allanites

7. Discussion

Allanite are most common REE minerals occurring in the deposit and surrounding rocks [2,7]. In some polished sections the concentration of allanite reaches 1 to 5% by volume (e.g. sample no. M5, S4, S9 – massive ores). The REE is present also in monazite, chevkinite, aeschynite, bastnäsite, apatite, pyrochlore [2, 9, 27], titanites and uraninite [20]. The average content of ΣREE in uraninites is relatively high (4.58 wt%) [11]. But they are rarely observed in the ores, and their influence on the total volume of REE in the deposit is negligible. In the massive sulphide, allanite concentrations reach up to several vol%, and epidote up to 5 vol% [7]. However, the bulk chemical data (Tab. 2) show that the average content of ΣREE is low – 701 ppm. This value corresponds roughly to 0.28% of allanite in volume.

According to Gas'kov et al. [2] epidote is dominate mineral in some sections and can also contain certain amounts of REE. Author WDS measurements of epidote (15 analyses) show elevated amounts of erbium (0.069 %) which is not observed in the investigated allanites (Fig.11), but it is visible on Fig. 5 showing REE pattern of host rocks.

The two different allanite populations have also been documented through routine microscopic observation of ore. The polished surface of low REE allanite (second population) is smoother, and this mineral is also characterised by lower reflectivity. Difference of these allanite populations is clearly observed in the amounts of Al_2O_3, CaO and total iron oxide (Tab. 3a, 3b). The average concentration of CaO and Al_2O_3 in first population is 13.9 wt% and 17.5 wt% respectively, while in the second one these oxides are 15.6 wt% and 19.3 wt% respectively (Tab. 3a, 3b). The amounts of SiO_2 in both populations are comparable. The total Fe oxides in first population is 21.7 wt% and in second one is 18.4 wt% in average. These values classify the investigated minerals as ferriallanite [29, 30]. The average concentration of La and Ce in the first population are 9.16 wt% and 13.8 wt%, in the second one is 6.73 wt% and 9.96 wt% respectively (Tab. 4a, 4b). Therefore cerium and lanthanum are dominating in allanite and the ratio Ce/La in both allanite populations varies from 1.48 to 2.32 so the considered allanite can be name as Ce-La-ferriallanite. The presence of two different allanite compositions is also visible on quantitative WDS compositional maps (Fig. 9Al - 9Fe). The allanite outer rim is younger. Different tints in the grey colour show mosaic textures of allanite crystals. The rim surrounding some allanite grains can be interpreted as an epitaxial allanite overgrowth from solutions with decreasing REE content during the final crystallisation phase. The chemical variability could be related to coupled substitution of REE^{3+} and Fe^{2+} by Ca^{2+} and Fe^{3+} ($REE^{3+} + Fe^{2+} \leftrightarrow Ca^{2+} + Fe^{3+}$) [7]. Statistical parameters calculated separately for the two populations of allanites show low values of standard deviation (Std.) and coefficient of variability (V) for all the major elements (Tabs. 3a, 3b, 4a and 4b). Higher variability of both the V and St.d. parameters are recorded for most of the minor constituents (Tabs. 3a, 3b, 4a and 4b). The correlations calculated for the basic elements in the allanites show good Pearson correlation between CaO, Al_2O_3, FeO and low correlation of SiO_2 vs ΣREE_2O_3 (Fig. 10A-10D). The negative correlation of CaO and Al_2O_3 vs ΣREE might suggest replacement of both cations by the REE during hydrothermal alteration, and recrystallization. The relation between total REE and Ca+(Fe3+)+Al expressed in apfu [29] for the WDS analyzed points of the two allanite populations is presented on the Fig.12, which indicates clearly difference between them.

Based on the replacement model proposed in publications by Li and Zhou [8], and Li et al. [9] the mass balance calculations are difficult in the case of hydrothermal processes. Ce-chevkinite, described in detail in the above mentioned publications, contains high total REE and TiO_2, and low total Fe and SiO_2, and a total absence of alumina. In the vicinity of allanite grains no Ti-oxides are observed, and replacement textures are commonly lacking. Based on these observations, it can be suggested, that crystallisation of the allanites and chevkinite took place during different stages of the deposit development. The first population of allanite (older) was formed during the early stages of alteration (841-836 Ma) (stage II) while the second one (younger) was established during the later hydrothermal processes (stage III) [3,20]. Temperature 355ºC let to explain position of second allanite stage [27]. This stage is documented also by the presence of sulphide inclusions within the altered allanite grains (Fig. 6F). The major volume of allanite is correlated with the precipitation of magnetite [27]. Association of both second allanite and magnetite minerals has been confirmed also in the mentioned above publications (575-430 Ma) [20]. This age is also confirmed by presence of REE within the magnetite [20]. Moreover, the second crystallization stage of uraninite is much younger and was dated 82-42 Ma [20]. Uraninites of this stage also contain substitutions of REE, and their chondrite normalized patterns of REE have significantly strong positive Eu and Lu anomaly in comparison with that in the older ones [20], but both allanite populations confirmed a presence of different stages and possible late

crystallization of REE containing mineral phases [20, 31, 32]. The patterns of REE of the two populations of alanites (Fig. 11) are similar themselves, however the second population has well visible negative Ce anomaly. Both populations are characterized with positive Ho, Tb and Lu anomalies. Differences in REE patterns of the host rocks (Fig. 5) and separately allanites (Fig. 11) can also suggested fluids circulation during time that results in chemical composition of both allanite populations. However, the REE patterns in the Fig. 5 are smooth. It is connected with REE broad dispersion in the host rocks, which took place during hydrothermal alteration. Hydrothermal alteration of the host rocks was happened during the cooling of fluids responsible for ions transportation and minerals crystallization. Temperature of 355ºC might be an initial temperature of the final crystallization of minerals which were recognized as a polymetallic stage.

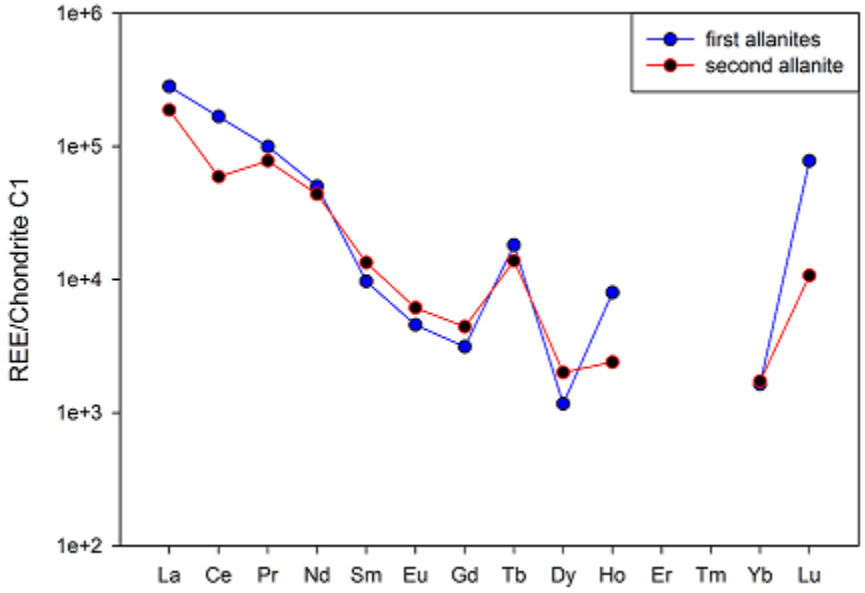

Fig.11. The REE pattern of two allanite groups

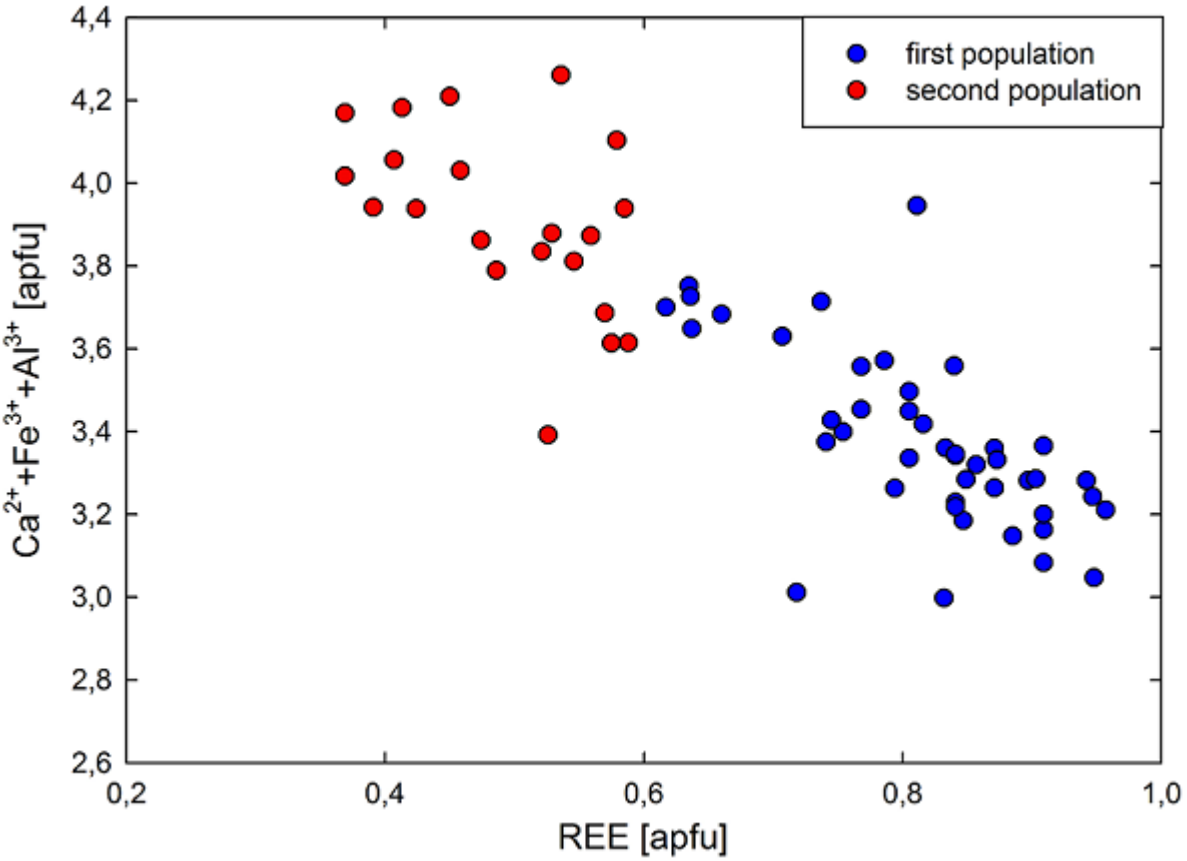

Fig. 12 ΣREE (apfu) versus $Ca+Fe^{3+}$ + Al (apfu) based on selected WDS point analyses.

7. Conclusions

Up to now, all the studies related to the Sin Quyen deposit have described petrological details concerning alteration processes based on the following replacement reactions chevkinite → allanite—aeschenite and bastnäsite, monazite → fluorapatite and allanite [2, 6, 31]. Chevkinite is occurring in a significantly small quantity [31] in comparison with the common allanite, and in addition, the other reaction mentioned above played a less important role.

Allanites are the major carriers of the REE metals. The differences in chemical composition clearly document the presence of two populations of allanites. The first is characterised by a higher total REE_2O_3 content at a level of 20 wt% to 27 wt% and lower CaO and Al_2O_3 but higher Fe (Tab. 3a, 3b). The chemical composition of the second ferriallanite group has a low total REE_2O_3 content, which ranges from 14 to 20 wt% (Tab. 4b). In addition, negative correlations have been noted between two pairs of major compositions of the allanite: CaO and REE_2O_3, R= –0.85 (Fig. 10A) and Al_2O_3 – REE_2O_3, R= -0.79 (Fig. 10B). A positive correlation was only noted for the FeO – REE_2O_3, R= 0.76 (Fig. 10C). A relatively weak correlation (R= 0.60) is observed for the pair SiO_2-REE_2O_3 (Fig. 10D). Apart from silica, all the major elements show a bi-modal distribution clearly visible on histograms (Fig. 13A – 13D). Silica, having a comparable amounts in both populations, the uni-modal characteristic (Fig. 13E) and very low coefficient of variability (4.1 and 3.7, rf. Tab. 3a and 3b), characterizes a more stable element in the allanite structure. All these correlations confirm the presence of two populations of allanite phases characterised by variable chemical composition. The visible differences between two allanite population is clearly seen in the relation of $Ca+Fe^{3+}$+Al and ∑REE expressed in apfu (Fig. 12). Additionally these differences were also clearly visible in Raman spectra [32]. Variability in the chemical composition of the

allanites can also suggest substitutions expressed as: $REE^{3+} + Fe^{2+} = Ca^{2+} + Fe^{3+}$ and $REE^{3+} + Fe^{2+} = Ca^{2+} + Al^{3+}$ [33]. A similar model was postulated following experiments carried out by [34]. The conclusion can therefore be drawn that the allanite minerals could be precipitated during different stages of the formation of the deposit.

Funding: This research received no external funding

Acknowledgement: The work was financially supported by the UST-AGH Krakow, Grants no 11.11.140.161 and 11.11.140.645 and University of Mining and Geology (UMG), Hanoi, Vietnam, Grant no. 01/2012/HD-HTQTSP. The authors are grateful to G. Kozub MSc and A. Włodek MSc from the Critical Elements Laboratory FGGEP UST-AGH Krakow for the WDS analyses and to T. Ćwiertnia MSc for preparation of the graphics. We also would like to thank the anonymous reviewer as well as prof. Phan Trong Trinh from Vietman Academy of Science and Technology for their valuable remarks.

Conflict of Interest: The authors declare no conflicts of interest. The funders had no role in the design of the study, in the collection and interpretation of data, in the writing of the manuscript, and in the declaration to publish the results.

Table 4a. WDS concentrations [wt%] of rare earth elements in the first population of the allanite

Nr	La_2O_3	Ce_2O_3	Pr_2O_3	Nd_2O_3	Sm_2O_3	Eu_2O_3	ΣLREE	Gd_2O_3	Tb_2O_3	Dy_2O_3	Ho_2O_3	Yb_2O_3	Lu_2O_3	ΣHREE	ΣREE	ΣLREE/ ΣHREE
1	5.89	9.89	1.04	2.84	0.21	b.d.l.	19.86	0.03	0.09	0.03	0.02	0.01	0.01	0.173	20.04	115
2	6.77	10.2	0.99	2.07	0.10	b.d.l.	20.16	0.09	0.04	b.d.l.	b.d.l.	0.02	0.02	0.178	20.34	113
3	6.86	10.0	0.86	2.15	0.18	0.06	20.16	0.17	0.07	0.05	b.d.l.	b.d.l.	0.04	0.330	20.49	61
4	6.94	10.2	0.89	2.36	0.20	0.04	20.66	b.d.l.	0.09	0.06	0.04	b.d.l.	b.d.l.	0.190	20.85	109
5	6.02	10.2	1.10	3.06	0.27	0.02	20.69	b.d.l.	0.07	b.d.l.	0.10	b.d.l.	b.d.l.	0.169	20.86	122
6	6.94	10.8	0.90	2.06	0.08	0.02	20.78	0.03	0.08	b.d.l.	b.d.l.	b.d.l.	b.d.l.	0.108	20.89	192
7	7.61	10.6	0.81	1.96	0.14	0.03	21.18	b.d.l.	0.05	0.05	0.02	0.01	0.01	0.135	21.32	157
8	4.43	10.6	1.34	4.56	0.50	0.06	21.44	b.d.l.	0.05	0.02	0.06	0.09	0.04	0.266	21.71	81
9	6.12	10.8	1.16	3.34	0.24	0.05	21.75	0.16	0.05	0.04	b.d.l.	b.d.l.	b.d.l.	0.245	22.00	89
10	6.78	10.8	1.08	3.17	0.25	0.04	22.14	b.d.l.	0.04	0.07	0.09	b.d.l.	b.d.l.	0.202	22.34	110
11	7.71	11.3	0.96	2.44	0.14	0.01	22.53	0.13	0.03	b.d.l.	b.d.l.	0.02	0.01	0.197	22.72	114
12	7.65	11.9	1.06	2.38	0.15	b.d.l.	23.19	b.d.l.	0.10	b.d.l.	b.d.l.	0.01	b.d.l.	0.107	23.30	217
13	5.25	11.8	1.30	4.41	0.35	0.06	23.14	b.d.l.	0.07	0.04	0.04	0.09	b.d.l.	0.232	23.37	100
14	8.07	11.8	1.00	2.30	0.17	0.01	23.33	b.d.l.	0.02	0.02	0.05	b.d.l.	0.01	0.099	23.43	236
15	7.91	11.6	1.15	2.44	0.19	b.d.l.	23.33	0.09	0.09	0.02	b.d.l.	0.03	0.04	0.267	23.60	87
16	8.39	11.8	0.96	2.18	0.13	0.01	23.51	b.d.l.	0.10	0.04	0.03	0.04	b.d.l.	0.211	23.72	111
17	8.11	12.2	0.98	2.33	0.13	0.03	23.77	0.12	0.02	0.03	b.d.l.	0.02	0.01	0.203	23.97	117
18	8.18	10.3	1.13	3.60	0.56	0.10	23.86	0.10	0.05	0.03	b.d.l.	b.d.l.	b.d.l.	0.186	24.04	128
19	8.64	12.3	0.96	2.05	0.07	0.02	24.05	0.05	0.06	0.03	b.d.l.	b.d.l.	b.d.l.	0.131	24.18	184
20	8.46	12.1	1.03	2.38	0.13	b.d.l.	24.09	0.07	0.11	0.01	b.d.l.	b.d.l.	0.04	0.223	24.31	108
21	7.85	12.7	1.16	2.46	0.11	0.01	24.31	b.d.l.	0.06	b.d.l.	0.02	0.01	b.d.l.	0.099	24.41	246
22	8.58	12.1	1.11	2.43	0.13	b.d.l.	24.33	0.07	0.09	0.02	b.d.l.	b.d.l.	0.02	0.194	24.53	125
23	6.05	12.8	1.28	3.96	0.27	0.05	24.38	0.09	0.04	0.05	b.d.l.	0.02	0.01	0.207	24.58	118

24	8.62	12.2	1.04	2.55	0.08	0.04	24.52	0.03	0.07	b.d.l.	b.d.l.	b.d.l.	0.02	0.118	24.64	208
25	8.36	12.4	1.15	2.52	0.16	0.01	24.57	0.12	0.04	0.06	0.05	0.01	b.d.l.	0.280	24.85	88
26	8.65	12.7	1.07	2.23	0.05	0.02	24.73	0.01	0.09	b.d.l.	0.05	0.03	0.01	0.177	24.91	140
27	8.53	12.9	1.04	2.29	0.11	0.05	24.88	0.05	0.04	0.04	0.01	0.02	0.01	0.159	25.04	156
28	8.96	12.4	1.10	2.30	0.13	0.01	24.90	0.05	0.07	b.d.l.	b.d.l.	0.02	b.d.l.	0.133	25.04	187
29	9.02	12.4	0.94	2.55	0.11	0.04	25.05	0.08	0.05	b.d.l.	b.d.l.	0.02	0.01	0.159	25.20	158
30	8.81	12.5	1.06	2.46	0.14	0.03	24.99	0.03	0.12	b.d.l.	0.04	0.03	b.d.l.	0.229	25.22	109
31	8.96	12.7	1.04	2.22	0.17	0.02	25.08	0.09	0.08	b.d.l.	b.d.l.	b.d.l.	b.d.l.	0.164	25.24	153
32	8.76	12.8	1.05	2.39	0.10	0.01	25.06	0.06	0.06	b.d.l.	0.01	b.d.l.	0.05	0.182	25.24	138
33	8.79	12.8	1.09	2.30	0.11	0.01	25.07	0.11	0.02	0.02	0.01	0.03	b.d.l.	0.184	25.25	136
34	8.56	12.9	1.13	2.49	0.14	0.01	25.25	b.d.l.	0.07	0.02	0.05	b.d.l.	b.d.l.	0.139	25.39	182
35	9.08	12.6	1.02	2.47	0.14	b.d.l.	25.27	0.01	0.04	0.01	0.07	0.01	b.d.l.	0.131	25.40	193
36	8.78	13.0	1.11	2.31	0.10	b.d.l.	25.28	0.01	0.11	0.02	b.d.l.	b.d.l.	0.02	0.163	25.44	155
37	9.15	12.7	1.02	2.34	0.17	b.d.l.	25.37	0.06	0.05	0.03	b.d.l.	0.02	b.d.l.	0.156	25.53	163
38	9.15	13.0	0.98	2.29	0.01	0.02	25.42	b.d.l.	0.01	0.01	0.13	0.01	b.d.l.	0.145	25.57	175
39	8.88	12.8	1.21	2.44	0.13	0.01	25.48	0.08	0.09	0.07	0.01	b.d.l.	b.d.l.	0.243	25.72	105
40	6.80	13.4	1.36	3.73	0.25	0.03	25.53	b.d.l.	0.13	b.d.l.	0.06	0.02	0.05	0.257	25.79	99
41	9.16	13.0	1.08	2.53	0.09	0.01	25.83	0.06	0.05	0.02	b.d.l.	0.03	b.d.l.	0.157	25.99	165
42	6.90	13.6	1.39	3.80	0.17	0.02	25.88	b.d.l.	0.08	0.05	0.12	0.02	b.d.l.	0.253	26.14	102
43	8.97	13.5	1.08	2.54	0.13	0.02	26.20	0.03	0.07	0.04	b.d.l.	b.d.l.	0.01	0.148	26.34	177
44	7.97	13.4	1.29	3.27	0.16	0.03	26.11	b.d.l.	0.04	0.01	0.07	0.13	0.02	0.256	26.36	102
45	7.49	13.8	1.39	3.56	0.15	0.06	26.50	b.d.l.	0.13	0.01	b.d.l.	0.04	0.02	0.192	26.69	138
min	4.43	9.89	0.81	1.96	0.01	0.01	19.86	0.01	0.01	0.01	0.01	0.01	0.01	0.10	20.04	61.00
max	9.16	13.80	1.39	4.56	0.56	0.10	26.50	0.17	0.13	0.07	0.13	0.13	0.05	0.33	26.69	246.00
Av.	7.83	12.04	1.09	2.69	0.17	0.03	23.82	0.07	0.07	0.03	0.05	0.03	0.02	0.19	24.01	137.73
St. d.	1.16	1.10	0.14	0.64	0.10	0.02	1.85	0.04	0.03	0.02	0.03	0.03	0.01	0.05	1.85	43.84
V[%]	14.86	9.13	12.67	23.98	61.54	70.34	7.79	60.29	44.99	55.22	69.02	95.60	65.79	28.70	7.70	31.83

Table 4b. WDS concentrations [wt%] of rare earth elements in second population of the allanite

Nr	La_2O_3	Ce_2O_3	Pr_2O_3	Nd_2O_3	Sm_2O_3	Eu_2O_3	ΣLREE	Gd_2O_3	Tb_2O_3	Dy_2O_3	Ho_2O_3	Yb_2O_3	Lu_2O_3	ΣHREE	ΣREE	ΣLREE/ ΣHREE
1	4.43	6.95	0.56	1.66	0.16	0.04	13.8	0.11	0.04	0.08	b.d.l.	b.d.l.	0.06	0.280	14.08	49
2	4.98	6.95	0.67	1.56	0.11	0.01	14.3	0.04	0.08	0.06	0.01	b.d.l.	b.d.l.	0.197	14.48	72
3	4.58	7.26	0.70	1.90	0.23	0.05	14.72	0.04	0.04	b.d.l.	0.04	b.d.l.	0.01	0.126	14.85	117
4	3.81	7.05	0.77	2.62	0.32	0.02	14.6	0.13	0.04	0.09	0.03	b.d.l.	0.01	0.296	14.89	49
5	5.15	7.49	0.68	1.65	0.13	0.02	15.12	0.08	0.03	0.02	b.d.l.	0.04	0.01	0.172	15.30	88
6	5.04	7.61	0.75	1.57	0.12	b.d.l.	15.10	0.11	0.04	0.08	b.d.l.	b.d.l.	0.06	0.280	15.38	54
7	4.74	7.81	0.74	1.80	0.24	0.03	15.4	0.02	0.07	0.01	0.06	0.01	b.d.l.	0.162	15.53	95
8	4.30	7.95	0.87	2.93	0.32	0.07	16.43	0.12	0.07	0.07	0.02	b.d.l.	0.04	0.306	16.74	54
9	5.34	8.41	0.75	2.00	0.22	0.05	16.76	0.08	0.06	0.01	0.01	b.d.l.	0.01	0.164	16.93	102
10	5.76	8.54	0.68	1.96	0.12	0.05	17.11	0.02	0.07	b.d.l.	b.d.l.	0.03	0.01	0.129	17.24	133
11	5.45	8.58	0.89	2.04	0.22	0.01	17.19	0.13	0.07	b.d.l.	b.d.l.	0.03	0.08	0.316	17.51	54
12	4.86	8.62	0.85	2.75	0.27	0.01	17.37	0.13	0.05	0.08	b.d.l.	0.01	b.d.l.	0.268	17.64	65
13	4.84	8.56	0.97	2.93	0.29	0.07	17.66	0.02	0.05	b.d.l.	b.d.l.	0.01	0.03	0.110	17.77	161
14	3.98	8.41	1.09	3.46	0.41	0.03	17.38	0.28	0.08	b.d.l.	0.04	0.02	b.d.l.	0.420	17.80	41
15	6.13	9.57	b.d.l.	2.43	0.20	0.16	18.49	0.13	0.04	0.04	0.02	b.d.l.	b.d.l.	0.233	18.72	79
16	4.46	9.45	0.98	3.24	0.34	0.05	18.52	0.15	0.07	0.10	b.d.l.	0.02	b.d.l.	0.338	18.86	55
17	5.27	9.05	0.95	2.63	0.34	0.05	18.29	0.20	0.11	0.11	0.02	0.11	0.03	0.575	18.86	32
18	6.19	9.67	0.83	1.97	0.12	0.01	18.80	0.04	0.07	b.d.l.	b.d.l.	b.d.l.	0.02	0.136	18.93	138
19	5.06	9.11	1.03	3.17	0.34	0.02	18.73	0.24	0.05	0.09	b.d.l.	0.04	0.05	0.475	19.21	39
20	6.73	9.55	0.84	1.96	0.12	0.01	19.22	0.01	0.04	0.06	b.d.l.	0.05	b.d.l.	0.145	19.37	133
21	6.58	9.30	0.95	2.16	0.21	0.02	19.21	0.11	0.04	0.03	b.d.l.	0.01	b.d.l.	0.182	19.39	106
22	6.52	9.96	0.95	1.99	0.18	0.01	19.60	b.d.l.	0.08	0.02	0.06	b.d.l.	b.d.l.	0.155	19.75	126
23	5.46	9.73	1.11	3.04	0.27	0.07	19.67	0.08	0.04	0.04	0.04	b.d.l.	0.02	0.214	19.89	92

min	3.81	6.95	0.56	1.56	0.11	0.01	13.8	0.01	0.03	0.01	0.01	0.01	0.01	0.11	14.08	32
max	6.73	9.96	1.11	3.46	0.41	0.16	19.67	0.28	0.11	0.11	0.06	0.11	0.08	0.575	19.89	161
ave	5.2	8.5	0.8	2.3	0.2	0.04	17.2	0.1	0.1	0.1	0.0	0.0	0.0	0.2	17.4	84.9
Std.	0.8	1.0	0.1	0.6	0.1	0.0	1.8	0.1	0.0	0.0	0.0	0.0	0.0	0.1	1.8	37.7
V[%]	15.4	11.2	17.0	24.9	37.7	84.6	10.6	69.2	33.7	57.1	60.3	89.1	76.6	48.7	10.6	44.4

Notes: Sought but no detected: Er. Tm; Av.- average content; V- coefficient of variability; St. d. – standard deviation; b.d.l. – below detection limit

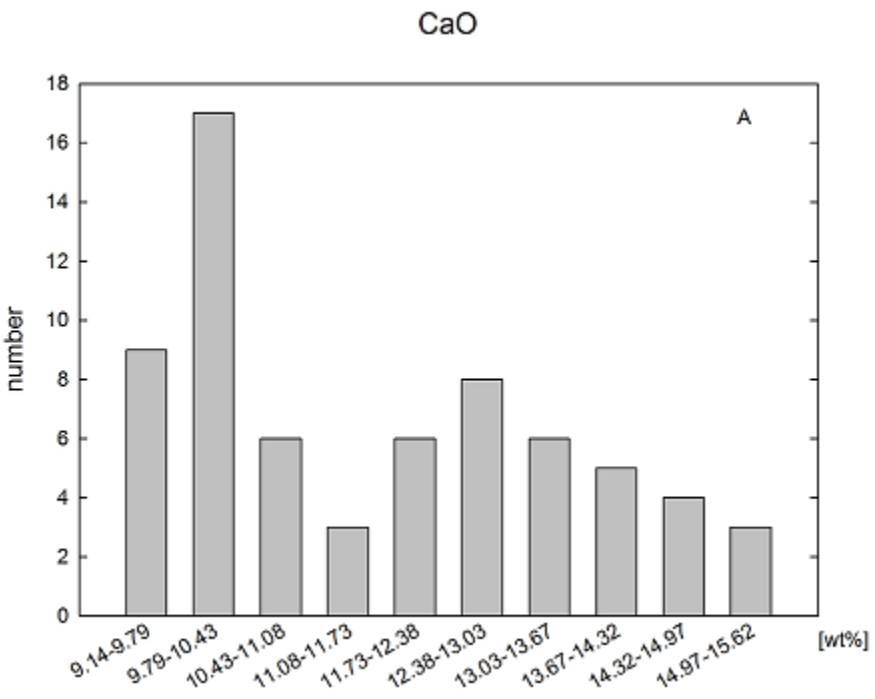

Fig. 13 A. Histograms of CaO in allanites.

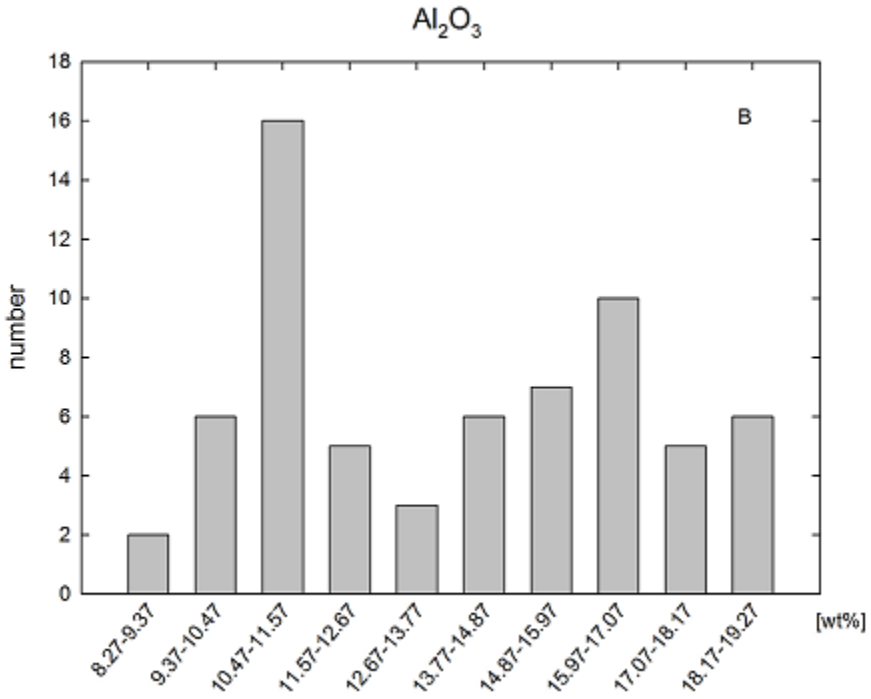

Fig. 13B**.** Histograms of Al_2O_3 in allanites

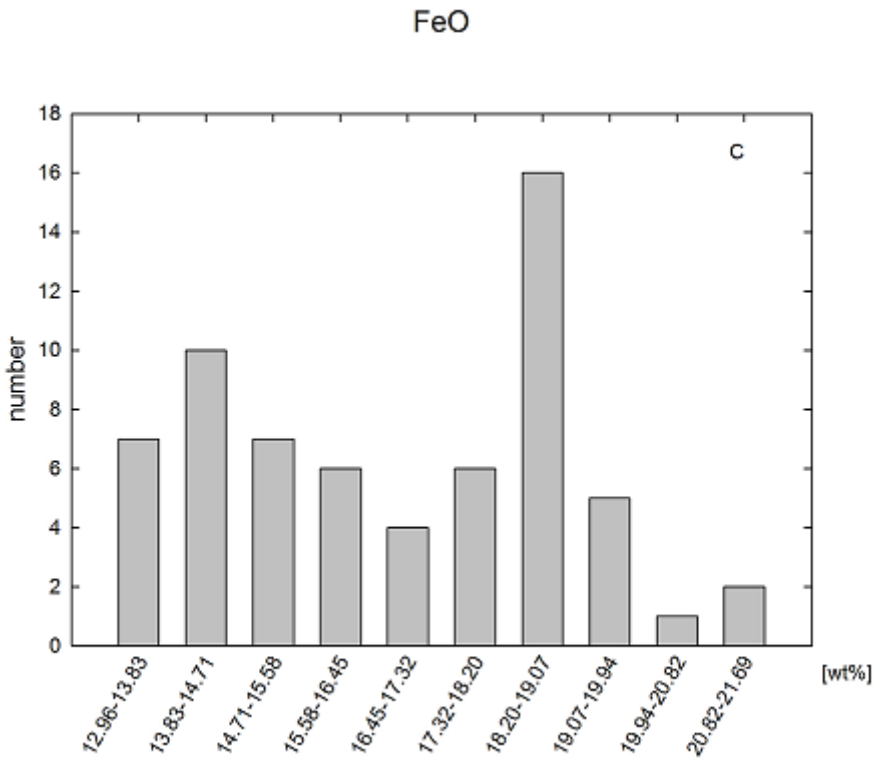

Fig. 13C. Histograms of FeO in allanites

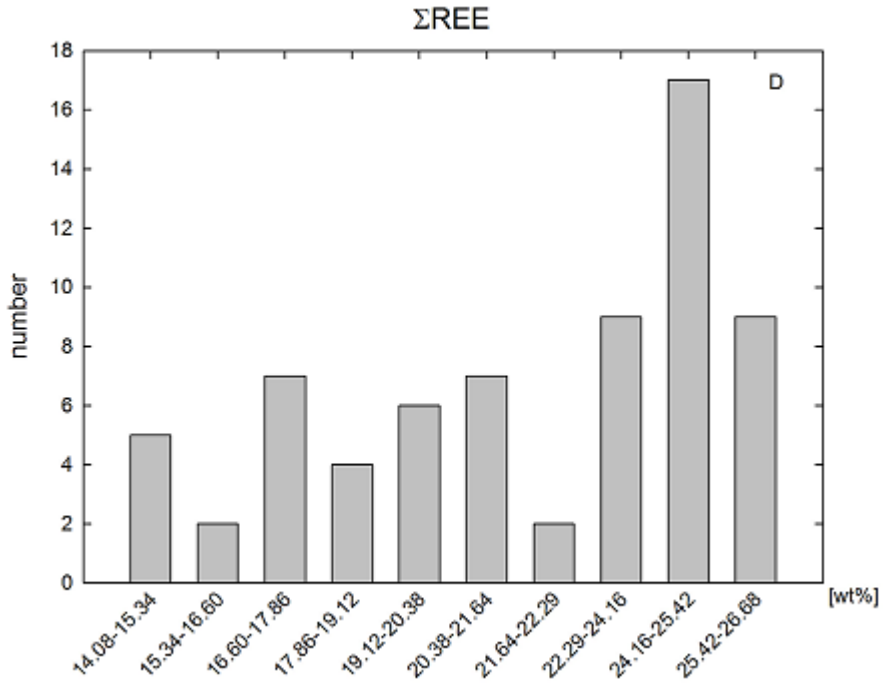

Fig. 13D. Histograms of ΣREE

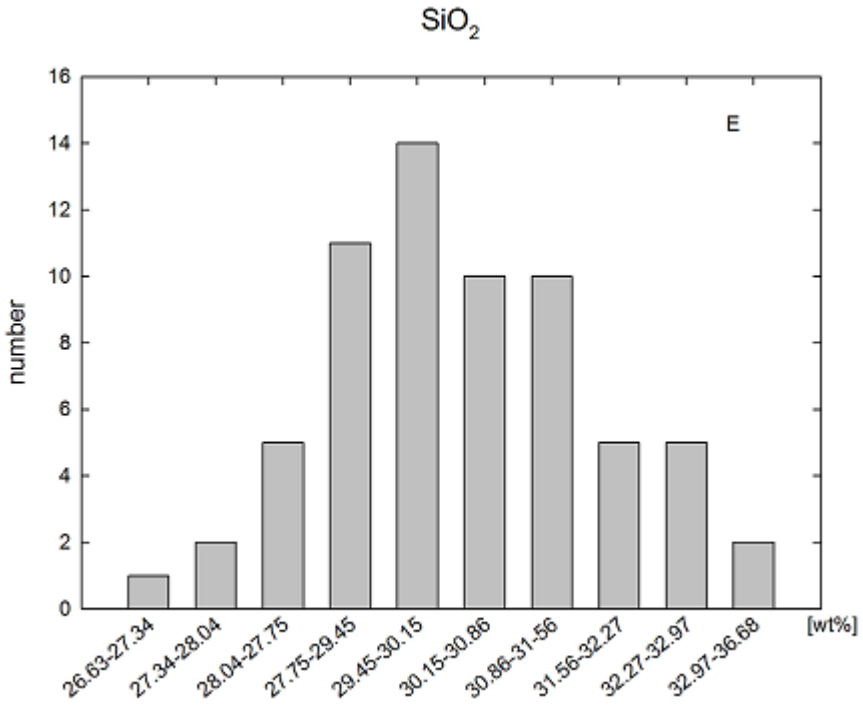

Fig. 13E**.** Histograms of SiO_2 in allanites

References

1. Pham. N.C.; Ishiyama. D.; Tran. T.A.; Sera. K. Mineralogical and geochemical characteristics of rare metals bearing Na Bop. Lung Hoai. Nason and Sin Quyen Base metal deposits. Northern Vietnam. *NMCC Annual Report*. **2011**. 18. 49-55.
2. Gas'kov. I.V.; Tran. T.A.; Tran. T.H.; Pham. T.D.; Nevolko. P.A.; Pham. N.C. The Sin Quyen Cu-Fe-Au-REE deposit (*northern Vietnam*) composition and formation conditions. *Russian Geology and Geophysics*. **2012**. 442-456.
3. Zhao. X.F.; Zhou. M.F. Fe–Cu deposits in the Kangdian region. SW China: a Proterozoic IOCG (iron-oxide–copper–gold) metallogenic province. *Mineralium Deposita*. **2011**. 46 (7). 731-747.
4. ESCAP. Report of Economic and Social Commission for Asia and the Pacific. **1990.**
5. Ta. V.D. Report of geological surveys and their results performed at the IOCG Sin Quyen deposit in Lao Cai. North Vietnam. Main Department of Geology of Vietnam. **1975**. 318 (in Vietnamese).
6. McLean. R.N. The Sin Quyen iron oxide-copper-gold-rare earth oxide mineralization of North Vietnam. *In Hydrothermal iron oxide copper-gold & related deposits: A global perspective*. Porter T.M. Ed.. PGC Publishing. Adelaide. **2001.** 293-301.
7. Ishihara. S.; Hideo. H.; Mihoko. H.; Pham. N.C.; Pham. T.D.; Tran. T.A. Mineralogical and chemical characteristics of the allanite-rich copper and iron ores from the Sin Quyen mine. northern Vietnam. *Bulletin of the Geological Survey of Japan*. **2011**. 62. 5/6. 197 – 209.
8. Li. X.C.; Zhou. M.F. Hydrothermal alteration of monazite-(Ce) and chevkinite-(Ce) from the Sin Quyen Fe-Cu-LREE-Au deposit. north-western Vietnam. *American Mineralogists*. **2017**. 102. 1525-1541.
9. Li. X.C.; Zhou. M.E.; Chen. W.T.; Zhao. X.F.; Tran. M.D. Uranium-lead dating of hydrothermal zircon and monazite from the Sin Quyen Fe-Cu REE-Au-(U) deposit. north-western Vietnam. *Mineralium Deposita*. **2018**. 53 (3). 399-416.
10. Pieczonka. J.; Piestrzyński. A.; Le. K.P.; Nguyen. D.C.; Jodłowski. P.; Doung. V.H. Rare Earth. radioactive and selected elements in the iron oxide copper gold Sin Quyen deposit in North Vietnam. In: *Second International Conference on Scientific Research Cooperation between Vietnam and Poland in Earth Sciences.* Bach Khoa Publishing House. Hanoi. **2015**. 331-353.
11. Pieczonka. J.; Piestrzyński. A.; Nguyen. D.C.; Le. K.P.; Duong. H.V. IOCG Sin-Quyen deposit. Lao Cai. N-Vietnam. *Mineral resources to discover. 14th Biennial SGA Meeting. Quebec. Canada*. **2017**. 955-959.
12. Faure. M.; Lepvrier. C.; Vuong. N.V.; Tich. V.V.; Lin. W.; Chen. Z. The South China block-Indochina collision: Where. when. and how? *Journal of Asian Sciences*. **2014**.79. 260-274.

13. LeLoup. P.H.; Tapponnier. P.; Lacassin. R. Discussion on the role of the Red River shear zone. Yunan and Vietnam in the continental extrusion of SE Asia. *Journal of Geological Society. London*. **2007**. 164. 1253-1260.
14. Tapponnier. P.; Lacassin. R.; Leloup. H.; Scharer. U.; Zhong. D.; Liu. X.; Ji. S.; Zhang. L.; Zhong. J. The Ailaoshan-Red river metamorphic belt: tertiary left-lateral shear between Indochina and South China. *Nature*. **1990**. 343. 431-437.
15. Roger. F.; Maluski. H.; Lepvrier. C.; Vu. V.T.; Paquette J.L. LA-ICPMS zircons U/Pb dating of Permo-Trassic and Cretaceous magmatism in Northern Vietnam – Geodynamical implications. *J. Asian Earth Sciences*. **2012**. 48. 72-82.
16. Lepvrier. C.; Maluski. H.; Van Vuong Nguyen; Roques. D.; Axente. V..;& Rangin. *C*. Indosinian NW-trending shear zones within the Truong Son belt (Vietnam). ^{40}Ar-^{39}Ar Triasic age and Cretaceous to Cenozoic overprints. *Tectonophysics*. **2008**. 283. 105-127.
17. *Carter*. A**.;** *Clift***.** P. D. Was the Indosinian orogeny a Triassic mountain building or a thermotectonic reactivation event?. Comptes Rendus. *Geosciences*. ***2008*.** 340. 83-93.
18. Tong-Dzuy. T.; Javier. P.; Ta Hoa. P. Fist suggest continental connections between the Indochina and South China blocks in Middle Devonian time. *Geology*.**1996**. 24. 571-574.
19. Liem N.V.; Dat N.P.; Dieu B.T.; Phai V.V.; Trinh P.T.; Vinh H.Q.; Phong T.V. Assessment of geomorphic processes and active tectonics in Con Voi mountain range area (Northern Vietnam) using the hypsometric curve analysis method. Vietnam J. Earth Sciences. **2016.** 38(2). 202-216.
20. Pieczonka J.; Chau N.D.; Piestrzyński A.; Phon L.K. Timing of ore mineralization using ore mineralogy and U-Pb dating. Iron Oxide Copper Gold Sin Quyen de posit. North Vietnam. *Geological Quarterly*. **2019**. 63(4). 861–874.
21. Pyle. J.M.; Spear. F.S.; Wark. D.A. Electron microprobe analysis of REE in apatite. monazite and xenotime: protocols and pitfalls. In *Reviews in Mineralogy and Geochemistry*. **2002**. 48. 337-362.
22. Seal. R. Sulphur isotope geochemistry of sulphide minerals. USGS Staff – Published Research. **2006**. 345.https://digitalcommons.unl.edu/usgsstaffpub/345
23. Ohmoto H.; Rye R.O. Isotopes of sulfur and carbon. In *Geochemistry of hydrothermal ore deposits*. 2nd. Barnes. H.L.. Ed. J Wiley and Sons. New York. **1979**. 509-567.
24. Dupuis. C.; Beaudoin. G. Discriminant diagrams for iron oxide trace element fingerprinting of mineral deposit types. *Mineralium Deposita*. **2011**. 46. 319-335.
25. Fengli. Y.; Yafei. W.; Shunfu. L.; Xiaofen. L.; Pengfei. G.; Jiannian. Z. Comparisons between the Zhuchong Fe-Cu Deposit in Anqing and the IOCG-type Deposits. *Acta Geologica Sinica*. **2014**. 88 (S2). 403-404.
26. Chen. W.T.; Zhou. M.F.; Gao. J.F.; Hu. R. Geochemistry of magnetite from Proterozoic Fe-Cu deposits in the Kangdian metallogenic province. SW China. *Mineralium Deposita*. **2015**. 50. 795-809.
27. Li. X.C.; Zhou. M.F. The nature and origin of hydrothermal REE mineralization in the Sin Quyen deposit. Northwestern Vietnam. *Economic Geology*. **2018**. 113 (3). 645-673.
28. Ngo. X.D.; Zhao. X.F.; Tran. T.H.; Deng. X.D.; li. J.W. Two episodes of REE mineralization of the Sin Quyen IOCG deposit. NW Vietnam. Ore Geology Reviews. **2020.** http://doi.org/10.1016/j.oregeorev.2020.103676.
29. Armbruster. T.; Bonazzi. P.; Akasaka. M.; Barmanec. V.; Chopin. C.; Giere. R., Heuss-Assbichler. S.; Liebscher. A; Menchetti. S.; Pan. Y.; and Pasero. M. Recommended nomenclature of epidote-group minerals. Eu. J. Mineral. **2006**. 18, 551-567.
30. http://webmineral.com/data/Ferriallanite-(Ce).shtml#.X8UMq2hKhaQ
31. Petrík. I.; Broska. I.; Lipka. J.; Siman. P. Granitoid Allanite-(Ce) substitution relations. redox conditions and REE distributions (on an Example of I-Type Granitoids. Western Carpathians. Slovakia). *Geolgia Carpathica*. **1995**. 46. 79–94.
32. Pieczonka. J.; Piestrzyński. A.; Nguyen. D.C.; Le. K.P.; Hao. D.V.; IOCG Sin-Quyen deposit. Lao Cai. N-Vietnam. Mineral resources to discover. 14th Biennial SGA Meeting. Quebec. Kanada. **2017**: 955-959.
33. Belperio. A.; Flint. R.; Freeman. H. Predominent Hill: A hematite dominated. iron oxide copper-gold system. *Economic Geology*. **2007**. 102. 1499-1510.
34. Budzyń. B.; Harlov. D.E.; Kozub-Budzyń. G.A.; Majka. J. Experimental constraints on the relative stabilities of the two systems monazite-(Ce) – allanite-(Ce) – fluor apatite and xenotime-(Y) – (Y.HREE)-rich epidote – (Y.HREE)-rich fluor apatite. in high Ca and Na-Ca environments under P-T conditions of 200–1000 MPa and 450–750 °C. *Mineralogy and Petrology*.**2017**. 111. 183–217.